Bulletin of the Earthquake
Research Institute
Vol. 45 (1967), pp. 749-783

40. A Long Wave around a Breakwater (Case of Perpendicular Incidence) [II].

By Takao Momoi,

Earthquake Research Institute.

(Read June 27, 1967.—Received June 30, 1967.)

Abstract

The present work is a continuation of the previous paper entitled "A Long Wave around a Breakwater (Case of Perpendicular Incidence) [I]". A governing equation of this problem is expressed by a velocity potential other than the long wave equation in the previous work. The calculated ranges of kd (k: the wave number of the incident waves; d: the half width of the breakwater gap) are 2.0 to 5.0 for the *RST* (resultant) waves and 0.1 to 5.0 for the *RD* (reflected and diffracted) waves. The variations of the waves for a change of kd are discussed for the nearby regions of a breakwater gap.

1. Introduction

Succeeding the previous work[1] with the same title (this paper will be referred to as paper I in the following), a long wave in the surrounding area of a breakwater gap is expounded numerically. In the present work, a theory is developed by using an expression of the velocity potential instead of the long wave equation employed in paper I.

2. Theory

2,1. Geometry of the Model Used.

The model used in this paper is exactly the same as that in paper I (see Fig. 1).

2,2. Governing Equation and Boundary Conditions.

Allowing for the extension of the theory to the waves of *medium wave-length*, a vertical component (z) is incorporated in the development of the theory. Assuming irrotational and infinitesimal motion in in-

1) T. Momoi, *Bull. Earthq. Res. Inst.*, **45** (1967), 91.

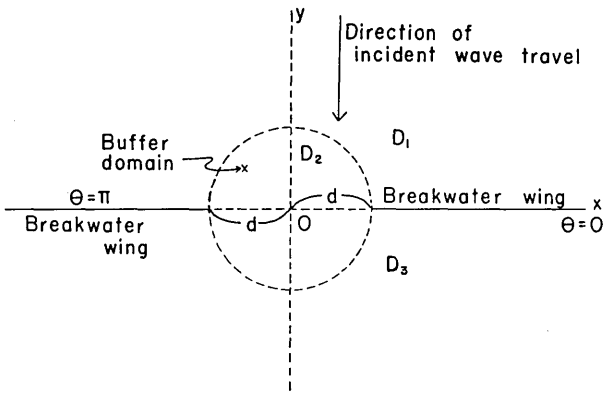

Fig. 1. Geometry of the used model.

compressible water, the velocity potential ϕ satisfies the equation (the equation of continuity)

$$\left(\frac{\partial^2}{\partial x^2}+\frac{\partial^2}{\partial y^2}+\frac{\partial^2}{\partial z^2}\right)\phi=0\,, \tag{1}$$

where x, y and z are cartesian coordinates, x- and y-axes are situated as shown in Fig. 1, z-axis positive upwards and the origin of the coordinates located at the undisturbed free surface of water.

Let ζ, g and t be, respectively, the elevation of water surface, the gravity constant and the time variable. ζ is expressed (from the relation of energy) as

$$\zeta=\frac{1}{g}\left(\frac{\partial\phi}{\partial t}\right)_{z=0}. \tag{2}$$

On the other hand, we have, as a kinematical condition,

$$\frac{\partial\zeta}{\partial t}=-\left(\frac{\partial\phi}{\partial z}\right)_{z=0}. \tag{3}$$

From (2) and (3), the surface condition for a velocity potential becomes

$$\frac{\partial^2\phi}{\partial t^2}+g\cdot\frac{\partial\phi}{\partial z}=0 \quad \text{at} \quad z=0\,. \tag{4}$$

Let H be the depth of water. The bottom condition is

$$\frac{\partial\phi}{\partial z}=0 \quad \text{at} \quad z=-H\,. \tag{5}$$

As far as the boundary condition at the rigid wall is concerned, we have

$$\left.\begin{aligned} &\frac{\partial\phi}{\partial y}=0 \quad \text{at} \quad (y=0,\ |x|>d) \\ \text{or} \\ &\frac{\partial\phi}{\partial\theta}=0 \quad \text{at} \quad (\theta=0 \text{ and } \pi,\ |x|>d)\ . \end{aligned}\right\} \tag{6}$$

The above condition denotes that the horizontal component of velocity of water particle disappears at the rigid boundary. In (6), θ is the azimuthal component of cylindrical coordinates (r, θ, z), r and θ being horizontal and z positive upwards.

Following the previous work (paper I), incident waves are assumed to be periodic ones in this paper, with an angular frequency ω. Then the velocity potential ϕ is expressed as

$$\phi=\phi' e^{-i\omega t}\ , \tag{7}$$

where $e^{-i\omega t}$ is the periodic time factor and only the real part of (7) has physical meaning (t is the time variable).

Substitution of (7) into (1), (4), (5) and (6) yields

$$\left(\frac{\partial^2}{\partial x^2}+\frac{\partial^2}{\partial y^2}+\frac{\partial^2}{\partial z^2}\right)\phi'=0\ , \tag{1'}$$

$$\left(-\omega^2+g\frac{\partial}{\partial z}\right)\phi'=0 \quad \text{at} \quad z=0\ , \tag{4'}$$

$$\frac{\partial\phi'}{\partial z}=0 \quad \text{at} \quad z=-H\ , \tag{5'}$$

$$\left.\begin{aligned} &\frac{\partial\phi'}{\partial y}=0 \quad \text{at} \quad (y=0,\ |x|>d) \\ \text{or} \\ &\frac{\partial\phi'}{\partial\theta}=0 \quad \text{at} \quad (\theta=0 \text{ and } \pi,\ |x|>d)\ . \end{aligned}\right\} \tag{6'}$$

In the following, the prime (′) of ϕ' is omitted, unless otherwise stated.

Under the assumption that the separation of variables is possible, the above equation and conditions become

$$\left(\frac{\partial^2}{\partial x^2}+\frac{\partial^2}{\partial y^2}+k^2\right)\phi_{xy}=0\ , \tag{8}$$

$$\left.\begin{aligned} &\frac{\partial \phi_{xy}}{\partial y}=0 \quad \text{at} \quad (y=0,\ |x|>d) \\ &\text{or} \\ &\frac{\partial \phi_{xy}}{\partial \theta}=0 \quad \text{at} \quad (\theta=0 \text{ and } \pi,\ |x|>d)\ , \end{aligned}\right\} \tag{9}$$

where

$$\phi=\phi_{xy}\cosh k(z+H) \tag{10}$$

and k is an *eigenvalue* of Airy's relation

$$\omega^2=gk\tanh kH\ . \tag{11}$$

In the above, ϕ_{xy} denotes a function of x and y only.

2,3. Incident Wave.

Since the incident waves are assumed as being periodic ones which invade perpendicular to the breakwater wings (see Fig. 1), these forms are expressed as

$$\left.\begin{aligned} &\phi_0 e^{-i\omega t-iky}\cosh k(z+H) \\ &\text{in complete form} \\ &\text{or} \\ &\phi_0 e^{-iky}\cosh k(z+H) \end{aligned}\right\} \tag{12}$$

when the time factor $e^{-i\omega t}$ is omitted.

The former of the above expressions of the incident waves, of course, satisfies the equation (1) and the boundary conditions (4) and (5) (for the latter the equation (1′) and the conditions (4′) and (5′) are referred to). In the above, ϕ_0 is the amplitude of the velocity potential of the incident waves.

2,4. Formal Solutions.

If one substitutes ζ for ϕ_{xy} in (8) and (9), the forms of the equation and the boundary condition in this work are found to be exactly the same as those in paper I ((3) and (5) in paper I), so that the formal solution in the previous work are useful in the development of the theory in this work. Therefore, using the results of paper I ((8) to (10) in paper I), the formal solutions are expressed as (for the domains $D_j(j=1, 2, 3)$, refer to Fig. 1):

in the domain D_1,

$$\phi_{xy}^{(1)} = 2\phi_0 \cos ky + \sum_{m=0}^{\infty} \phi_1^{(2m)} H_{2m}^{(1)}(kr) \cos 2m\theta \ ; \tag{13}$$

in the domain D_2,

$$\phi_{xy}^{(2)} = \sum_{m=0}^{\infty} \{\bar{\phi}_2^{(2m)} J_{2m}(kr) \cos 2m\theta + \phi_2^{(2m+1)} J_{2m+1}(kr) \sin (2m+1)\theta\} \ ; \tag{14}$$

in the domain D_3,

$$\phi_{xy}^{(3)} = \sum_{m=0}^{\infty} \phi_3^{(2m)} H_{2m}^{(1)}(kr) \cos 2m\theta \ ; \tag{15}$$

where $\phi_{xy}^{(j)}$ $(j=1, 2, 3)$ are the factors (relevant to x and y or r and θ) of the velocity potentials in the domains D_j $(j=1, 2, 3)$, which are related to the velocity potentials ϕ_j $(j=1, 2, 3)$ in the domains D_j $(j=1, 2, 3)$ as follows:

$$\phi_j = \phi_{xy}^{(j)} \cosh k(z+H) \tag{16}$$

and where $\phi_1^{(2m)}$, $\bar{\phi}_2^{(2m)}$, $\phi_2^{(2m+1)}$ and $\phi_3^{(2m)}$ $(m=0, 1, 2, \cdots)$ are the unknown factors to be determined by the boundary conditions between the adjacent domains.

2,5. Conditions between Adjacent Domains.

As far as the conditions between the adjacent domains are concerned, we have two conditions available, one of which is the continuity of pressure and the other the continuity of water particles. Such conditions are as follows:

$$\left.\begin{aligned} &\phi_{xy}^{(2)} = \phi_{xy}^{(1)} \\ &\frac{\partial \phi_{xy}^{(2)}}{\partial r} = \frac{\partial \phi_{xy}^{(1)}}{\partial r} \end{aligned}\right\} \quad \text{for} \quad (r=d,\ 0<\theta<\pi) \tag{17}$$

and

$$\left.\begin{aligned} &\phi_{xy}^{(2)} = \phi_{xy}^{(3)} \\ &\frac{\partial \phi_{xy}^{(2)}}{\partial r} = \frac{\partial \phi_{xy}^{(3)}}{\partial r} \end{aligned}\right\} \quad \text{for} \quad (r=d,\ \pi<\theta<2\pi) \ , \tag{18}$$

where d is the half-width of the breakwater gap.

In the above, the factor $\cosh k(z+H)$ is omitted, for the depth of

water is uniform so that the factor does not contribute to the above conditions.

If the substitution of ζ_j $(j=1, 2, 3)$ for $\phi_{xy}^{(j)}$ $(j=1, 2, 3)$ in (17) and (18) is made, these conditions are found to be identical in form with those of (11) and (12) in paper I.

2,6. Infinite Simultaneous Equations.

Since the formal solutions (13) to (15) and the conditions (17) and (18) have, as already mentioned, the same forms with those in paper I, a further development of the theory goes along the same lines with those in paper I. Therefore, following the procedures in paper I, we have arrived at the following infinite simultaneous equations:

$$\frac{2}{\pi}\varepsilon_n \sum_{m=0}^{\infty} \frac{(2m+1)}{(2m+1)^2-(2n)^2} \begin{Bmatrix} J_{2m+1}(kd) \\ J'_{2m+1}(kd) \end{Bmatrix} \phi_2^{(2m+1)} + \begin{Bmatrix} H_{2n}^{(1)}(kd) \\ H_{2n}^{(1)\prime}(kd) \end{Bmatrix} \phi_3^{(2n)} = \varepsilon_n \begin{Bmatrix} J_{2n}(kd) \\ J'_{2n}(kd) \end{Bmatrix} \phi_0 \quad (n=0, 1, 2, \cdots), \tag{19}$$

which are referred to (28) in paper I.

In the above equations, the quantities in the wavy brackets are taken in the same order and

$$\varepsilon_n = \begin{cases} 1 & \text{for} \quad n=0 \\ 2 & \text{for} \quad n \geqq 1 . \end{cases}$$

In the derivation of (19),

$$\left.\begin{aligned} \bar{\phi}_2^{(2n)} &= \varepsilon_n \phi_0 \\ \phi_1^{(2n)} &= -\phi_3^{(2n)} \end{aligned}\right\} \tag{20}$$

are found, which correspond to (26) and (27) in paper I.

2,7. Simplified Forms of the Formal Solutions.

Using (20) and following the procedures in Section *2,6* in paper I, the formal solutions (13) to (15) are reduced to:

$$\phi_{xy}^{(1)}(r, \theta_1) = 2\phi_0 \cos ky - \phi_{xy}^{(3)}(r, \theta_3) \tag{21}$$

(refer to (31) in paper I),

$$\phi_{xy}^{(3)}(r, \theta_3) = \sum_{m=0}^{\infty} \phi_3^{(2m)} H_{2m}^{(1)}(kr) \cos 2m\theta_3 \tag{22}$$

(refer to (32) in paper I),

$$\phi_{xy}^{(2)}=\phi_0\cos ky+\sum_{m=0}^{\infty}\phi_2^{(2m+1)}J_{2m+1}(kr)\sin(2m+1)\theta \qquad (23)$$

(refer to (33) in paper I),

where $\theta_1=-\theta_3$ for $0<\theta_1<\pi$.

2,8. The $(2l+1)$ th Approximation.

As the second step of the method of the buffer domain (the first step is to express the given field by the orthogonal functions), the approximation is applied to the expressions of the buffer domain in order to make the infinite simultaneous equations finite ones.

In the same manner as that in paper I, setting $J_m(kr)$ $(r\leqq d)$ for $m>2l+1$ $(l=0, 1, 2, \cdots)$ equal to zero (retaining $J_m(kr)$ for $m\leqq 2l+1$), the infinite simultaneous equations (19) are reduced to:

$$\frac{2}{\pi}\varepsilon_n\sum_{m=0}^{l}\frac{(2m+1)}{(2m+1)^2-(2n)^2}\begin{Bmatrix}J_{2m+1}(kd)\\ J'_{2m+1}(kd)\end{Bmatrix}\phi_2^{(2m+1)}$$
$$+\begin{Bmatrix}H_{2n}^{(1)}(kd)\\ H_{2n}^{(1)\prime}(kd)\end{Bmatrix}\phi_3^{(2n)}=\varepsilon_n\begin{Bmatrix}J_{2n}(kd)\\ J'_{2n}(kd)\end{Bmatrix}\phi_0 \quad \text{for} \quad 0\leqq n\leqq l \qquad (24)$$

and

$$\frac{2}{\pi}\varepsilon_n\sum_{m=0}^{l}\frac{(2m+1)}{(2m+1)^2-(2n)^2}J_{2m+1}(kd)\phi_2^{(2m+1)}+iY_{2n}(kd)\phi_3^{(2n)}=0$$
$$\text{for} \quad n\geqq l+1, \qquad (25)$$

where (24) and (25) are referred to (42) and (43) in paper I.

When the approximation of the Bessel function described above is employed, the infinite series of the solution (23) is reduced to the finite ones up to the terms $m=l$, which correspond to (41) in paper I with the substitution of ζ_2, ζ_0 and $\zeta_2^{(2m+1)}$ for $\phi_{xy}^{(2)}$, ϕ_0 and $\phi_2^{(2m+1)}$ respectively in this work.

Now since the expressions (21)-(23) and (24)-(25) are reduced to (31)-(33) and (42)-(43) in paper I with appropriate substitutions, the factors $\phi_{xy}^{(j)}$ $(j=1, 2, 3)$ of the velocity potentials ϕ_j $(j=1, 2, 3)$ are readily computed with the aid of an electronic computer, following the same procedures as those in paper I.

2,9. Identification of the Notations.

In the development of the theories in paper I and the present study, we have employed different governing equations, so that the identification of two notations is made in the following.

Since the velocity potential (in this case, a complete form (7) is considered) is related with the wave height through the surface condition (2), the expression

$$\zeta = \frac{-i\omega}{g}\phi \qquad (z=0)$$

is readily derived (the primes of ζ' and ϕ' are omitted, where $\zeta = \zeta' e^{-i\omega t}$).

Substituting (10) into the above equation, the relation

$$\zeta = \frac{-i\omega}{g}\phi_{xy} \cosh kH \tag{26}$$

is obtained.

The incident waves are, in particular, reduced to (by use of (12))

$$\zeta_{in} = \frac{-i\omega}{g}\phi_0 e^{-iky} \cosh kH \,,$$

where ζ_{in} is the wave height of the incident waves (time factor is omitted).

Setting down

$$\zeta_0 = \frac{-i\omega}{g}\phi_0 \cosh kH \,, \tag{27}$$

the above expression becomes

$$\zeta_{in} = \zeta_0 e^{-iky} \,. \tag{28}$$

This expression implies that (27) is referred to the amplitude of the height of the incident waves employed in paper I.

Dividing (26) by (27), one obtains

$$\frac{\zeta}{\zeta_0} = \frac{\phi_{xy}}{\phi_0} \,. \tag{29}$$

Following the procedures described in Section *2,8*, ϕ_{xy} can be calculated, so that the relative amplitude (the amplitude divided by that of the incident waves) begins to be known through (29).

3. Numerical Calculations and Discussions

The computer programs employed in the calculations are the same as those in the previous work with a few improvements of the subroutine

of the Bessel functions, which enable us to compute the simultaneous equations with many more unknowns.

The calculations were carried out for *RST* waves (which are an abbreviation of *r*esul*t*ant waves) for $kd=2.0$, 3.0, 4.0, 5.0 and for *RD* waves (which are an abbreviation of *r*eflected and *d*iffracted waves) $kd=0.1$, 1.0, 2.0, 3.0, 4.0, 5.0.

RST waves are expressed by the left-hand sides of (13) to (15), while *RD* waves are the waves excluding the incident ones and are described by

$$\phi_{rd}^{(j)}=\phi_{xy}^{(j)}-\phi_0 e^{-iky} \qquad (j=1, 2)\ , \tag{30}$$

in the domains D_j $(j=1, 2)$ respectively. In the above, $\phi_{rd}^{(j)}$ is a factor (relevant to the horizontal components x and y) of the velocity potential of *RD* waves, $\phi_{xy}^{(j)}$ given by (13) or (14), and the last term $\phi_0 e^{-iky}$ is a factor of the velocity potential relevant to the incident waves. From (30), *RD* waves are purely reflected and diffracted waves excluding the invading ones.

3,1. Check of Convergence.

In this section, a check of convergence of the approximated theories is carried out through the calculations of the amplitude of the *RST* waves in six directions, i.e., $\theta=0+\varepsilon$, $\pi/4$, $\pi/2$ and $0-\varepsilon$, $-\pi/4$, $-\pi/2$ (ε is an infinitesimal) for $kd=3.0$, 4.0 and 5.0 (for convergence of the approximated theory of $kd=2.0$, readers should refer to paper I). These curves are shown in Figs. 2 to 7. According to these figures, the agreements of the curves of the theories for the stated approximations are found to be fairly good except for the part near $r/d=1.0$, in which slight disagreements are found. Such disagreements of the curves are attributed to the deficiency of the cited approximations, as already mentioned in paper I.

In drafting the pictures showing the overall variations of the waves in later sections, these disagreements are smoothed out appropriately.

3,2. Variations of Amplitude in Typical Directions.

Referring to Figs. 2 to 7, the variations of the amplitude along the directions of $\theta=0\pm\varepsilon$, $\pm\pi/4$ and $\pm\pi/2$ are discussed.

In the curves of the amplitude along the forward wall of the breakwater (the curves stated by $\theta=0+\varepsilon$ in Figs. 2, 4 and 6), undulatory variations of the amplitude having $|\zeta|=2.0$ as the axis of the undulation are found, among which the first undulation is the greatest in amplitude.

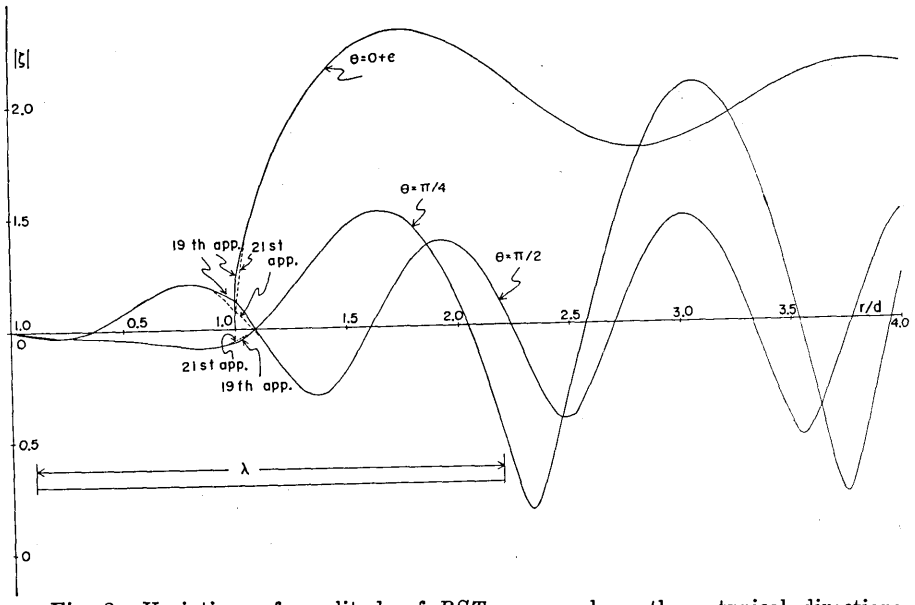

Fig. 2. Variations of amplitude of *RST* waves along three typical directions $\theta=0+\varepsilon$, $\pi/4$ and $\pi/2$ in the windward waters of the breakwater for $kd=3.0$ (this figure, and the five following ones, are depicted in large scale for the convenience of comparing with experiment).

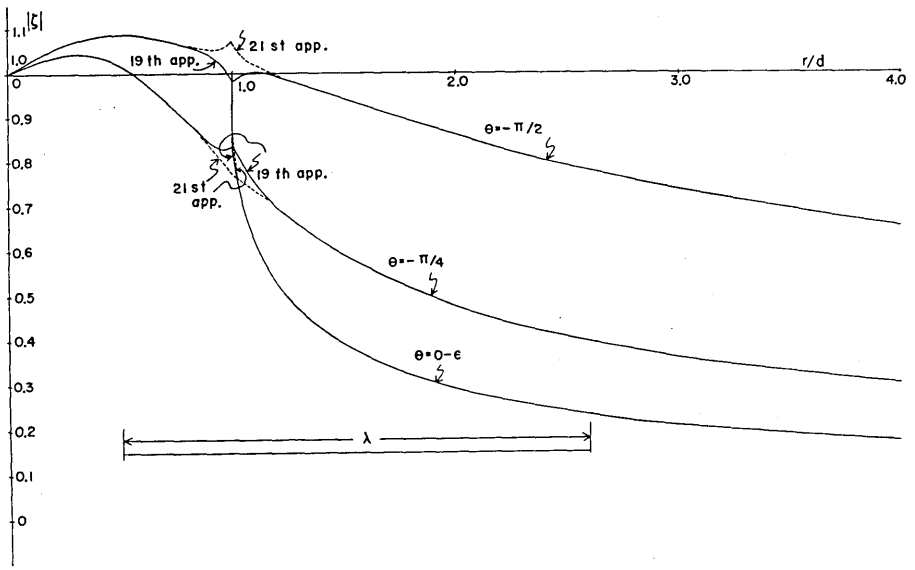

Fig. 3. Variations of amplitude of *RST* waves along three directions $\theta=0-\varepsilon$, $-\pi/4$, $-\pi/2$ in the leeward waters for $kd=3.0$.

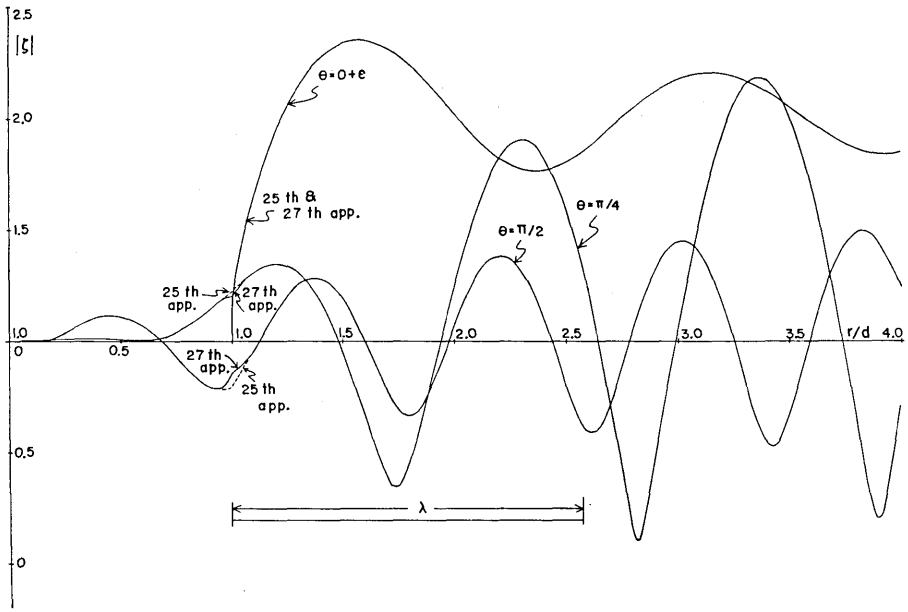

Fig. 4. Variations of amplitude of *RST* waves along three directions $\theta=0+\varepsilon$, $\pi/4$, $\pi/2$ in the windward waters for $kd=4.0$.

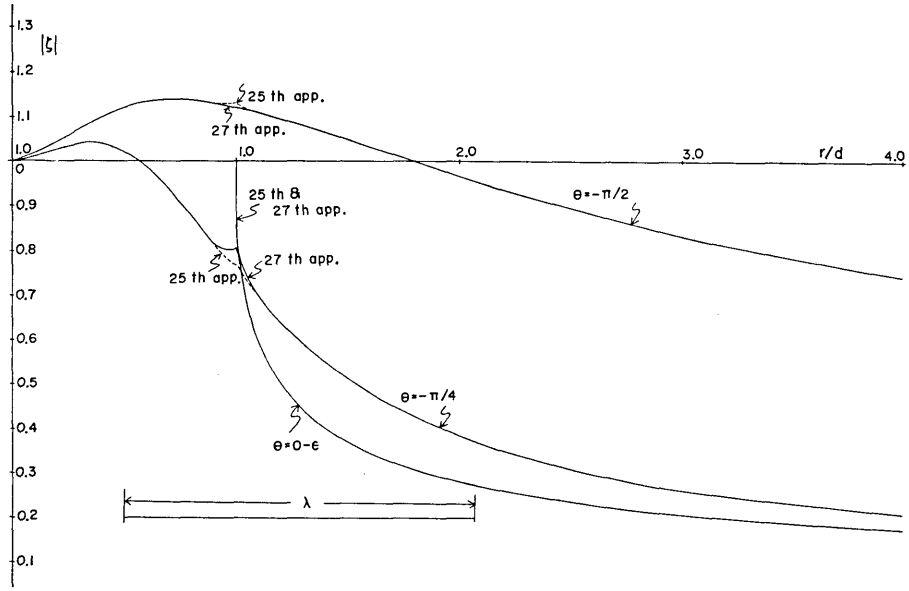

Fig. 5. Variations of amplitude of *RST* waves along three directions $\theta=0-\varepsilon$, $-\pi/4$, and $-\pi/2$ in the leeward waters for $kd=4.0$.

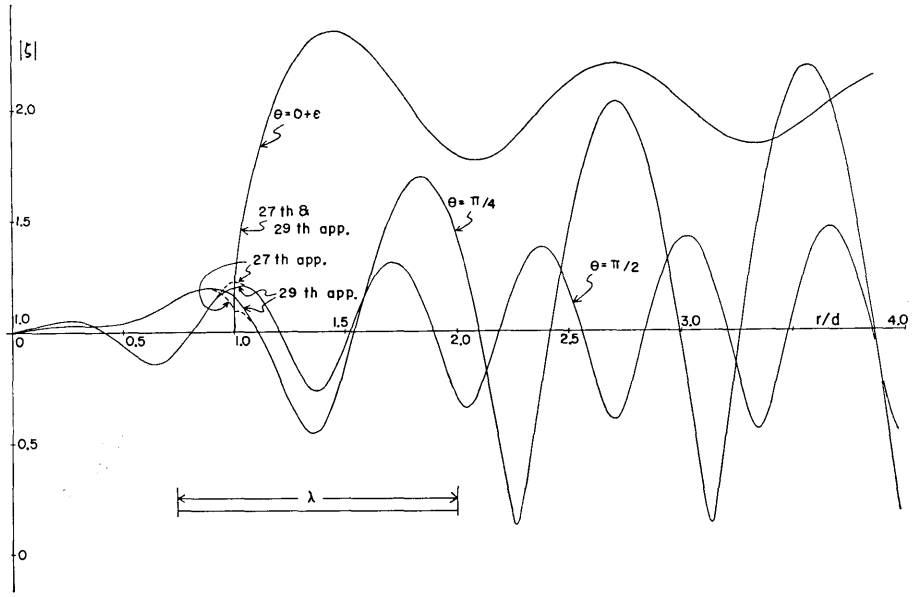

Fig. 6. Variations of amplitude of RST waves along three directions $\theta=0+\varepsilon$, $\pi/4$ and $\pi/2$ in the windward waters for $kd=5.0$.

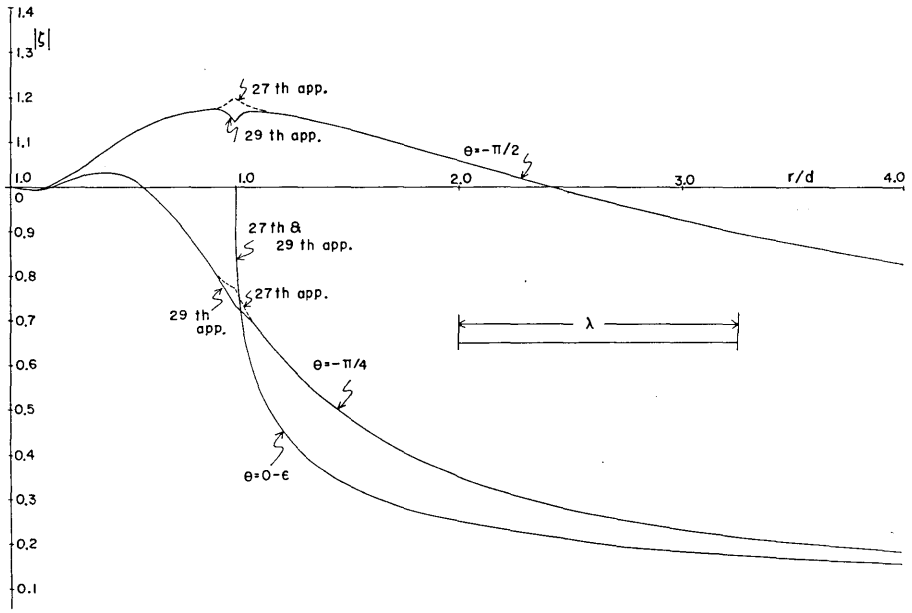

Fig. 7. Variations of amplitude of RST waves along three directions $\theta=0-\varepsilon$, $-\pi/4$ and $-\pi/2$ in the leeward waters for $kd=5.0$.

Such a phenomenon has already been noted in paper I with an explanation of the generation mechanism of such high waves. Comparing the scale of the wave-length λ of the incident waves (drawn in each figure for Figs. 2 to 7) and the variation of the amplitude, the above undulations are found to be repeated with a period of wave-length λ. When θ (the azimuthal component of the polar coordinates) increases from $0+\varepsilon$ to $\pi/4$ and $\pi/2$ (refer to the curves stated by $\pi/4$ and $\pi/2$ in Figs. 2, 4 and 6), the wave-length of the undulation of the amplitude diminishes. That is to say, the undulations are repeated with a wave-length of two-thirds of λ in the direction $\theta=\pi/4$ and with half the wave-length of λ in the direction $\theta=\pi/2$. Other than the variations of the amplitude along the forward wall ($\theta=0+\varepsilon$), the undulations along the directions $\theta=\pi/4$ and $\pi/2$ increase in amplitude as r increases.

Although the above-mentioned facts are found for the range $kd=3.0$ to 5.0, these facts have also been found for the range $kd=0.1$ to 2.0 in the previous work (paper I).

As far as the variations of the amplitude in the leeward waters of the breakwater are concerned (refer to Figs. 3, 5 and 7), the amplitude in general decreases as r increases except for the area near the gap of the breakwater. In a manner similar to that of paper I, the values of $|\zeta|$ at $r=\lambda+d$ in the leeward waters are tabulated in Table 1.

Table 1. The values of $|\zeta|$ at $r=\lambda+d$ in the leeward waters of the breakwater.

θ \ kd	3.0	4.0	5.0
$0-\varepsilon$	0.202	0.227	0.224
$-\pi/4$	0.350	0.299	0.306
$-\pi/2$	0.725	0.884	1.020

Inspection of Figs. 3, 5, 7 and Table 1 reveals that, when kd increases from 3.0 to 5.0, the directivity of the waves becomes more and more severe in the same way as that for the range of $kd=0.1$ to 2.0 in paper I. The ratios of the amplitudes in the directions $\theta=-\pi/2$ and $0-\varepsilon$ at a point $r=\lambda+d$ ($PD=|\zeta|_{\theta=-\pi/2}/|\zeta|_{\theta=0-\varepsilon}$) are as follows ($PD$ is an abbreviation of *P*arameter of *D*irectivity).

$$\left.\begin{aligned} PD=1.01 \quad &\text{for} \quad kd=0.1\,, \\ PD=1.06 \quad &\text{for} \quad kd=0.5\,, \end{aligned}\right\}$$

$$\left.\begin{aligned} PD&=1.26 \quad \text{for} \quad kd=1.0\,, \\ PD&=1.65 \quad \text{for} \quad kd=1.5\,, \\ PD&=2.25 \quad \text{for} \quad kd=2.0 \end{aligned}\right\} \tag{31}$$

and

$$\left.\begin{aligned} PD&=3.58 \quad \text{for} \quad kd=3.0\,, \\ PD&=3.89 \quad \text{for} \quad kd=4.0\,, \\ PD&=4.55 \quad \text{for} \quad kd=5.0\,. \end{aligned}\right\} \tag{32}$$

In the above, the first group of values is calculated from Table 1 in paper I, while the second group is computed from Table 1 in this paper. The value of PD is considered as implying the extent of the directivity of the waves. The values of PD arranged in (31) and (32) show an increase of the directivity of waves for the augmentation of kd.

According to the curves showing the variation of the amplitude in the direction $\theta=-\pi/2$ (the curves stated by $\theta=-\pi/2$ in Figs. 3, 5 and 7), the values of the amplitude $|\zeta|$ exceed once the unit value to take a maximum at a certain point apart from the breakwater gap and later on decrease monotonically, crossing the line $|\zeta|=1.0$. The above maximum point is in a sense moving away from the breakwater gap as kd increases from 3.0 to 5.0. Such an excess of the amplitude over 1.0 implies the appearance of the mound behind the breakwater gap. This inference will be ascertained in a later section which treats the overall variation of the amplitude around the breakwater gap.

3,3. Overall Variations of the Amplitude and Phase of RST Waves.

In this section, the behavior of the *RST* waves in the nearby region of the breakwater gap is explained for specified parameters $kd=2.0$, 3.0, 4.0 and 5.0. The pictures of the variations of the amplitude and phase are presented in Figs. 8(aw), 8(pw), 8(al), 8(pl) for $kd=2.0$, Figs. 9(aw), 9(pw), 9(al), 9(pl) for $kd=3.0$, Figs. 10(aw), 10(pw), 10(al), 10(pl) for $kd=4.0$ and Figs. 11(aw), 11(pw), 11(al), 11(pl) for $kd=5.0$, where the italic letters aw, pw, al and pl in the parentheses are the abbreviations, respectively, of the *a*mplitude of the waves in the *w*indward waters of the breakwater, the *p*hase in the *w*indward waters, the *a*mplitude in the *l*eeward waters and the *p*hase in the *l*eeward waters. Hence Fig. 8(aw), for instance, denotes the figure relevant to the amplitude variation of the *RST* waves in the windward sea of the breakwater for $kd=2.0$. The approximations employed in drafting the above pictures are the 11 th

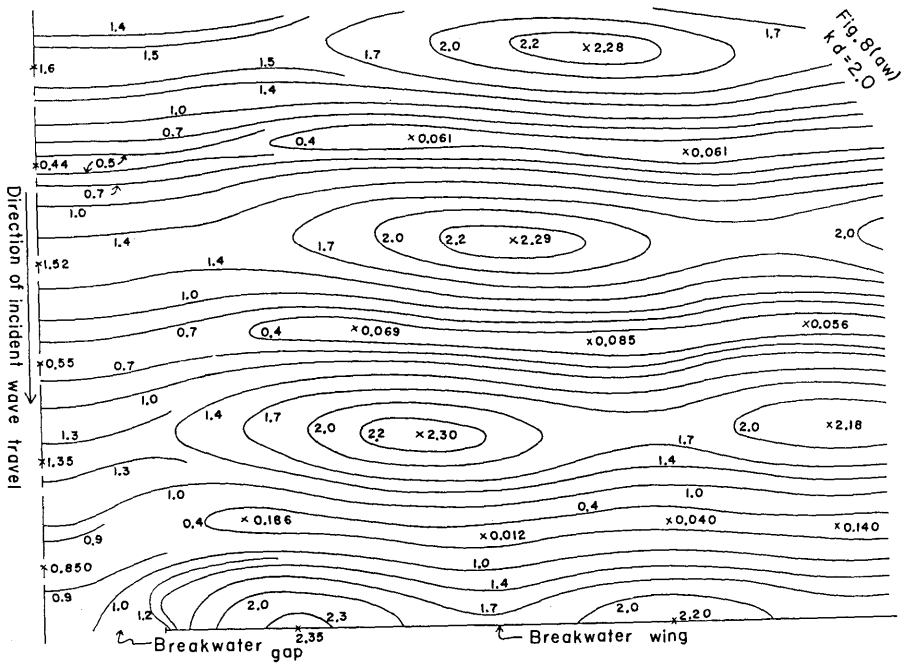

Fig. 8(*aw*). Overall variation of amplitude of *RST* waves in the windward waters of the breakwater for $kd=2.0$. The stated values in the figure denote those of $|\zeta/\zeta_0|$, normalized by the amplitude of the incident waves (=1.0). Since the variation is symmetric about the straight line perpendicular to the breakwater wing passing through the center of the breakwater gap, only the right-hand figure is depicted.

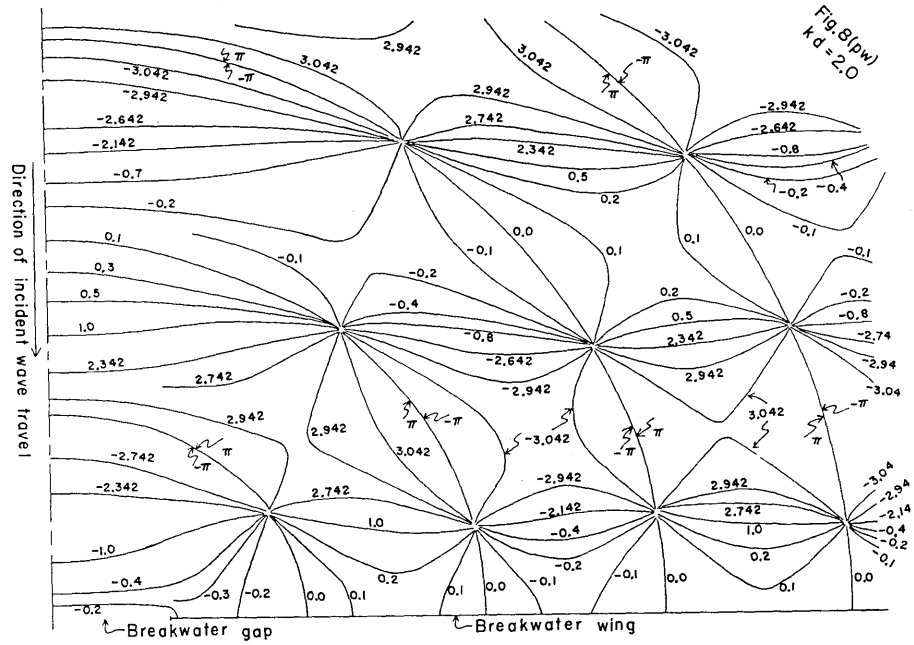

Fig. 8(*pw*). Overall variation of phase of *RST* waves in the windward waters for $kd=2.0$. The values stated in the figure denote arg ζ (which is calculated in the range $-\pi<\arg\zeta\leqq\pi$). Because of the symmetry, only the right-hand figure is depicted.

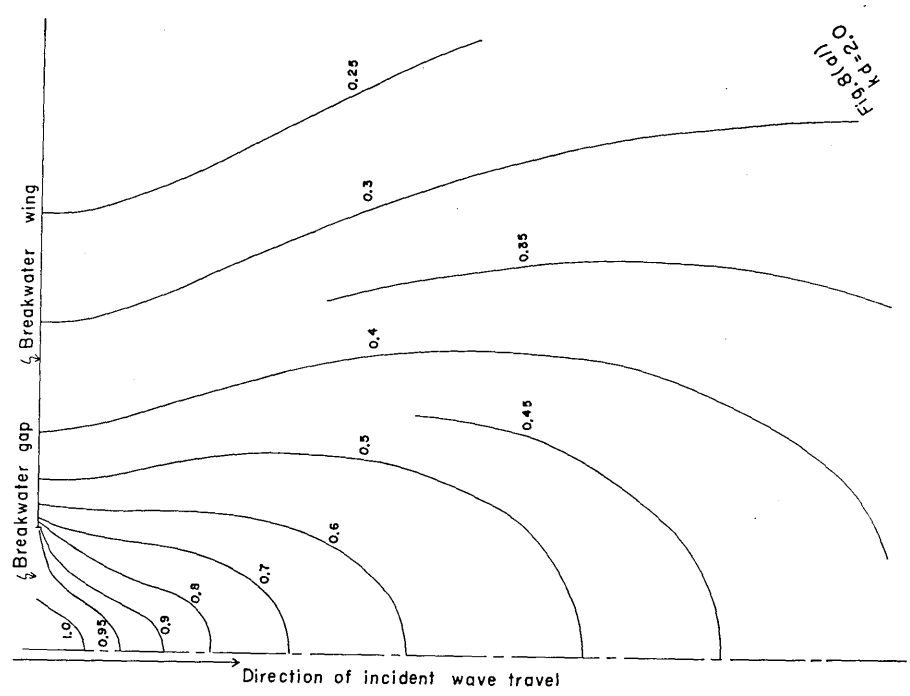

Fig. 8(*al*). Overall variation of amplitude ($|\zeta/\zeta_0|$) of *RST* waves in the leeward waters for $kd=2.0$. Because of the symmetry, only the right-hand figure is depicted.

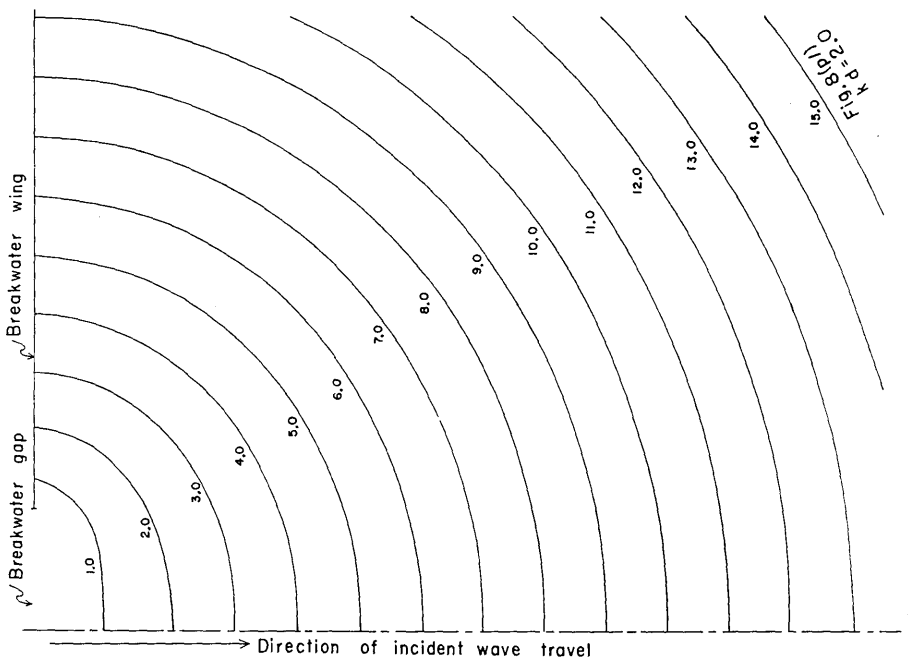

Fig. 8(*pl*). Overall variation of phase ($\arg\zeta$) of *RST* waves in the leeward waters for $kd=2.0$. Because of the symmetry, only the right-hand variation is retained.

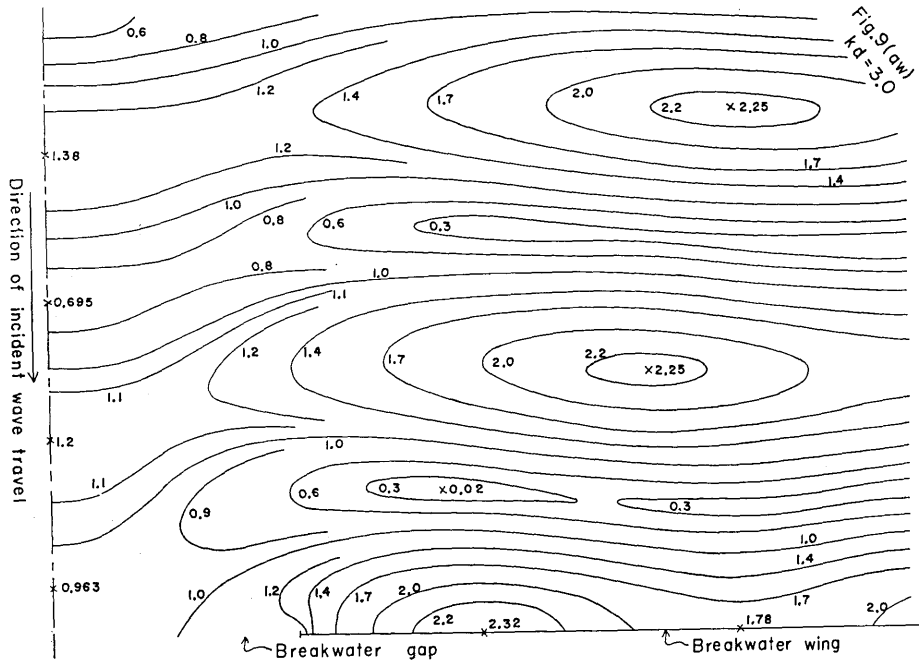

Fig. 9(*aw*). Overall variation of amplitude of *RST* waves ($|\zeta/\zeta_0|$) in the windward waters for $kd=3.0$. Owing to the symmetry, only the right-hand figure is depicted.

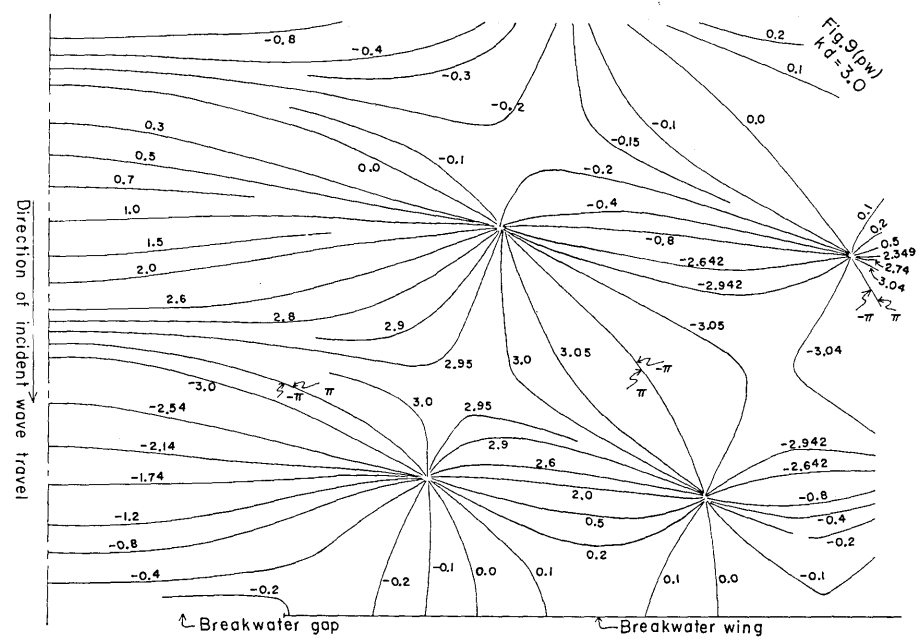

Fig. 9(*pw*). Overall variation of phase ($\arg\zeta$) of *RST* waves in the windward waters for $kd=3.0$. The values of $\arg\zeta$ are calculated in the range $-\pi<\arg\zeta\leqq\pi$. Owing to the symmetry, only the right-hand figure is depicted.

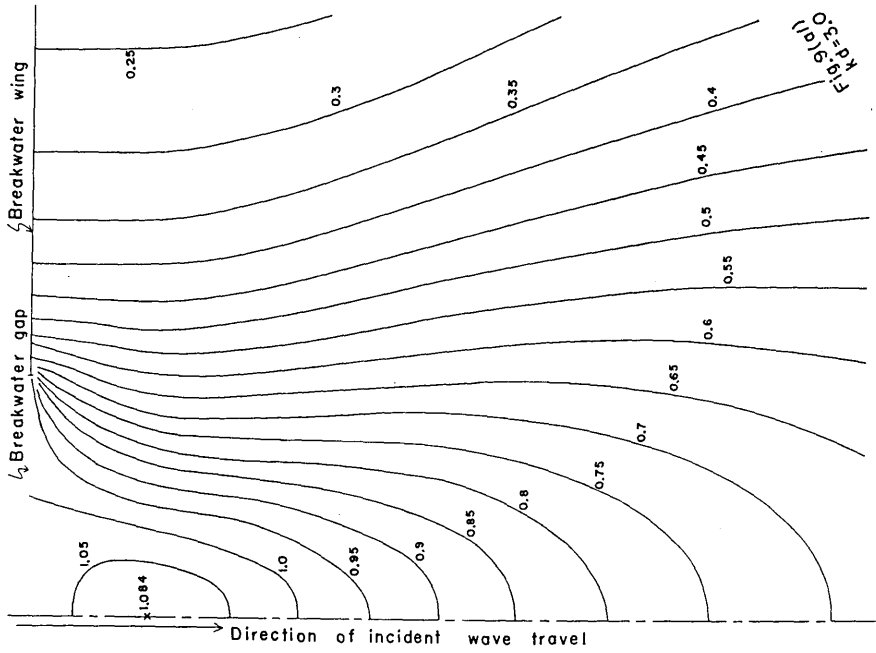

Fig. 9(*al*). Overall variation of amplitude ($|\zeta/\zeta_0|$) of *RST* waves in the leeward waters for $kd=3.0$. Only the right-hand figure is retained due to the symmetry.

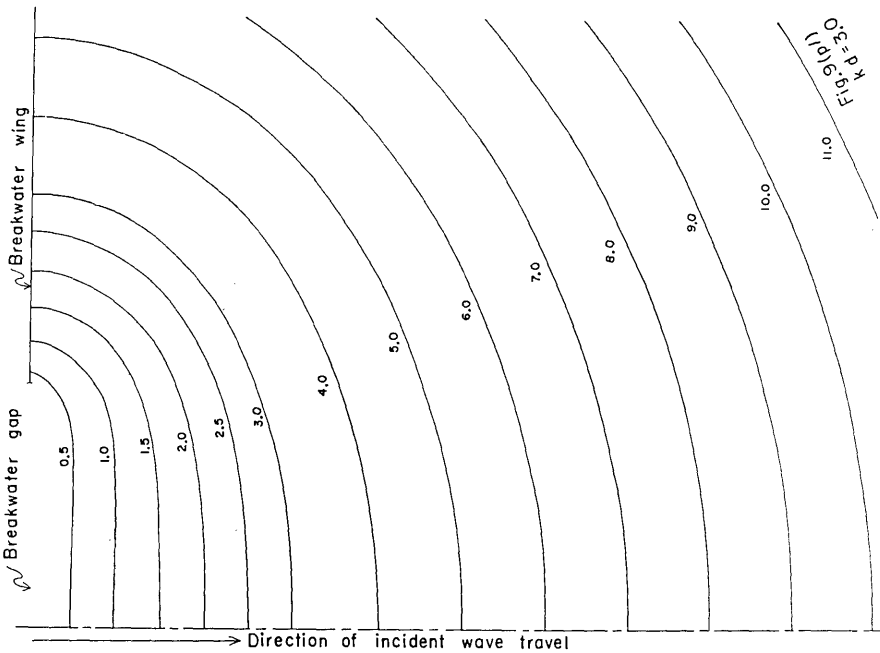

Fig. 9(*al*). Overall variation of phase (arg ζ) of *RST* waves in the leeward waters for $kd=3.0$. Only the right-hand figure is depicted.

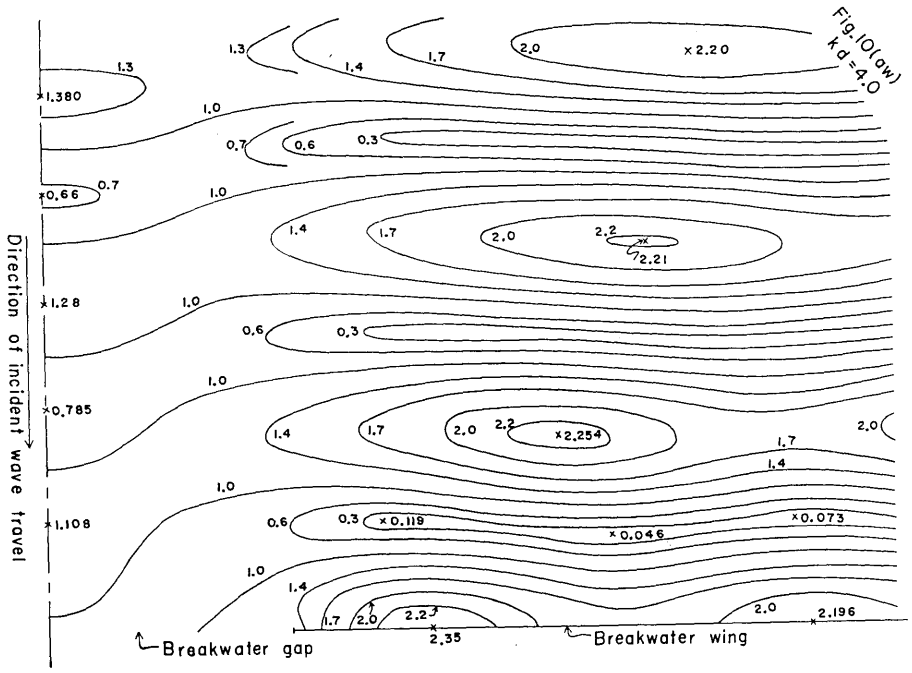

Fig. 10(*aw*). Overall variation of amplitude ($|\zeta/\zeta_0|$) of *RST* waves in the windward waters for $kd=4.0$. Only the half figure is depicted.

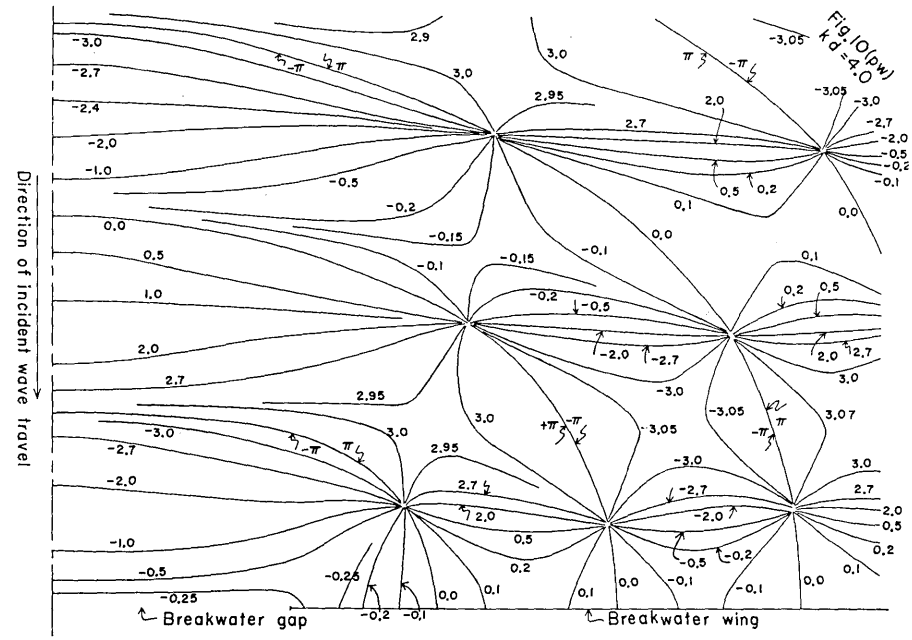

Fig. 10(*pw*). Overall variation of phase (arg ζ) of *RST* waves in the windward waters for $kd=4.0$. The values of arg ζ are calculated in the range $-\pi<\arg\zeta\leqq\pi$. Only the half figure is depicted.

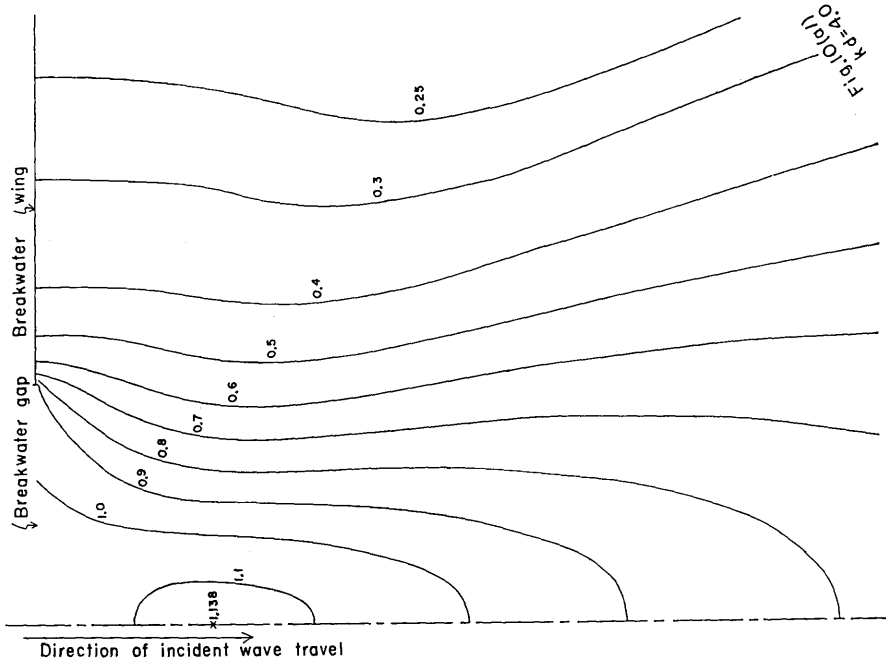
Breakwater wing
Breakwater gap
0.25
0.3
0.4
0.5
0.6
0.7
0.8
0.9
1.0
1.1
1.138
Direction of incident wave travel
Fig. 10(al). Overall variation of amplitude (|ζ/ζ0|) of RST waves in the leeward waters for kd=4.0. Only the half figure is retained.

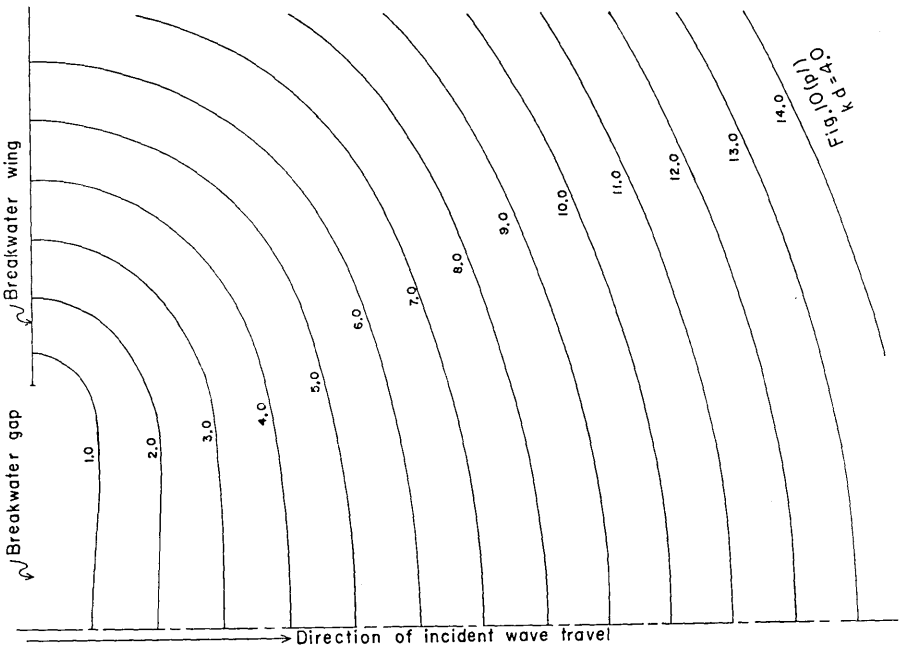
Breakwater wing
Breakwater gap
1.0
2.0
3.0
4.0
5.0
6.0
7.0
8.0
9.0
10.0
11.0
12.0
13.0
14.0
Direction of incident wave travel
Fig. 10(pl). Overall variation of phase (arg ζ) of RST waves in the leeward waters for kd=4.0. Only the half figure is depicted.

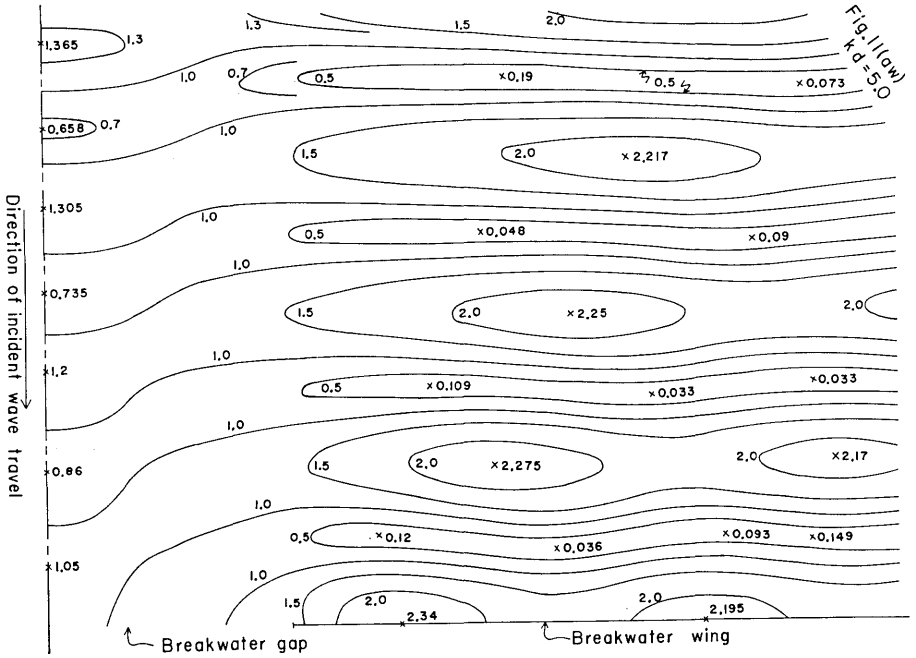

Fig. 11(*aw*). Overall variation of amplitude ($|\zeta/\zeta_0|$) of *RST* waves in the windward waters for $kd=5.0$. Because of the symmetry, only the right-hand variation is depicted.

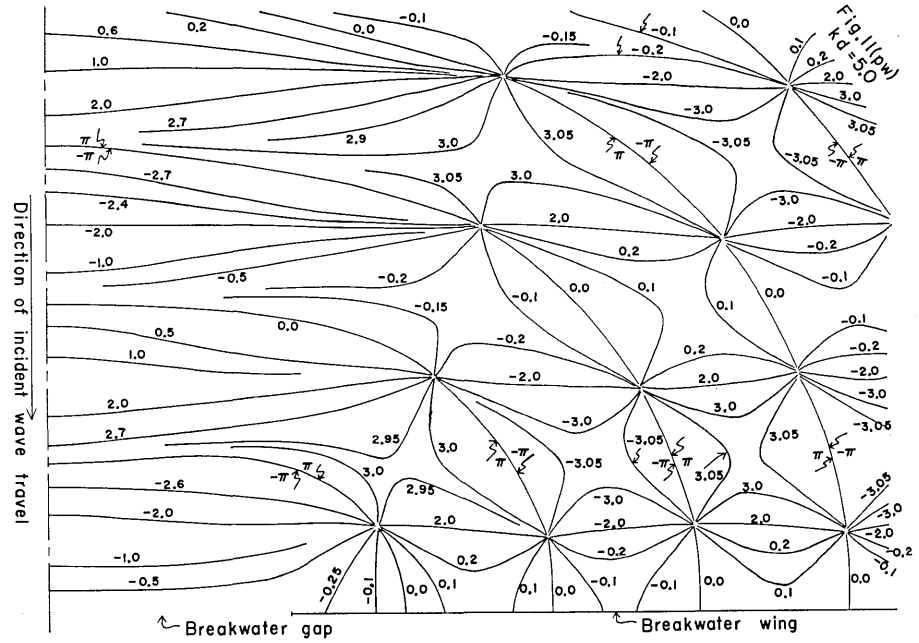

Fig. 11(*pw*). Overall variation of phase (arg ζ) of *RST* waves in the windward waters for $kd=5.0$. The values of arg ζ are taken in the range $-\pi < \arg\zeta \leqq \pi$. Only the half figure is depicted.

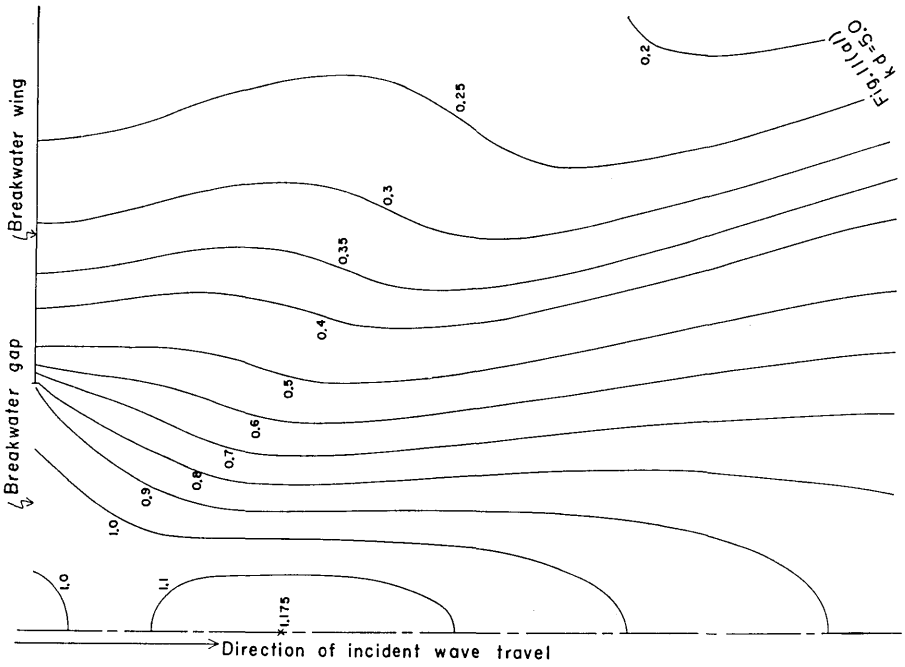

Fig. 11(d). Overall variation of amplitude ($|\zeta/\zeta_0|$) of *RST* waves in the leeward waters for kd=5.0. Only the half figure is retained.

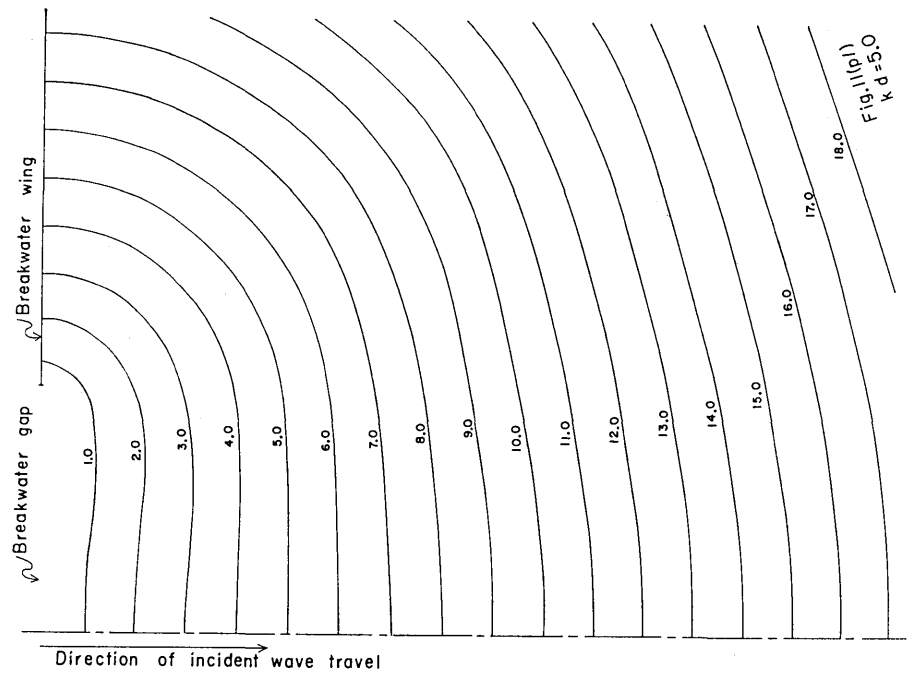

Fig. 11(p). Overall variation of phase (arg ζ) of *RST* waves in the leeward waters for kd=5.0. Only the half figure is retained.

approximation for $kd=2.0$ (Figs. 8(aw), 8(pw), 8(al) and 8(pl)), the 19 th approximation for $kd=3.0$ (Figs. 9(aw), 9(pw), 9(al) and 9(pl)), the 27 th approximation for $kd=4.0$ (Figs. 10(aw), 10(pw), 10(al) and 10(pl)), and the 29 th approximation for $kd=5.0$ (Figs. 11(aw), 11(pw), 11(al) and 11(pl)).

To begin with, mention is made of the variations of the amplitude in the windward waters. Referring to Figs. 8(aw), 9(aw), 10(aw) and 11(aw), the following facts are exposed.

When kd increases (the wave-length of the incident waves decreases as compared with the breakwater gap), a geometric shadow begins to be more definite owing to the growing nature of the directivity of the waves. That is to say, quasi-standing waves appear in the regions facing the breakwater wings, while, in the area in front of the breakwater gap, the undulatory variation of the amplitude is small compared with that in the former region as the result of the direct invasion of the incident waves towards the breakwater gap (refer to Fig. 12). In the latter region, small mounds and valleys appear nearly independent of the amplitude variation in the regions of the geometric shadow (see Fig. 13) with the contours of the amplitude bending down towards the

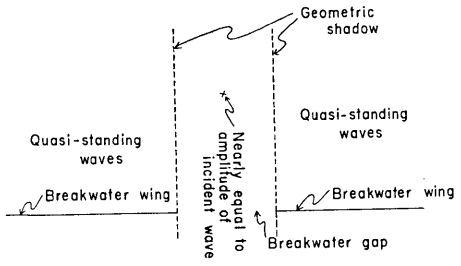

Fig. 12. Generation of the geometric shadow in the windward waters.

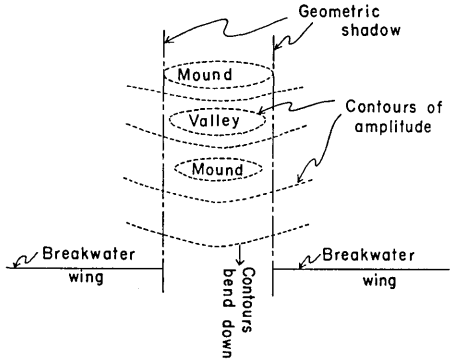

Fig. 13. Appearance of the independent variation of the amplitude in front of the breakwater gap.

leeward waters. A similar phenomenon was also found for the case of long waves around an estuary, of which a figurative explanation is given in Fig. 18 of the paper entitled "A Long Wave in the Vicinity of an Estuary [III]"[2]. Passing through four figures (Figs. 8(aw), 9(aw), 10(aw), and 11(aw)), high amplitudes exceeding twice the amplitude of the incident waves, as already noted in paper I, appear in the nearby area

2) T. MOMOI, *Bull. Earthq. Res. Inst.*, **44** (1966), 1009.

adjacent to the breakwater gap and in the offing facing the breakwater wings. The former is denoted by "HIGH I" and the latter by "HIGH II", "HIGH III" and so on in paper I. As described for the range of $kd=0.1$ to 1.0 in paper I, the amplitude in the part of "HIGH I" is also the largest among the above-mentioned high waves for the range of $kd=2.0$ to 5.0 in this work. The generation mechanisms of the above-mentioned two types of high waves denoted by "HIGH I" and "HIGH II", HIGH III", etc. are completely different. "HIGH I" is produced by a collision of the diverted waves towards the breakwater wing, while "HIGH II", "HIGH III", etc. are generated in the offing, being caused by an interference of the diverted waves reflected at the breakwater wing and the directly reflected waves (refer to Fig. 14). For the understanding of the above mechanism, the figures concerning the variation of phase (Figs. 8(pw), 9(pw), 10(pw) and 11(pw)) in the windward waters might be very helpful. Through all the figures relevant to the variation of the amplitude in the windward waters including the corresponding pictures in paper I, it is found that the part of the high waves referred to as "HIGH I" moves gradually to the corner of the breakwater wing (refer to Fig. 15).

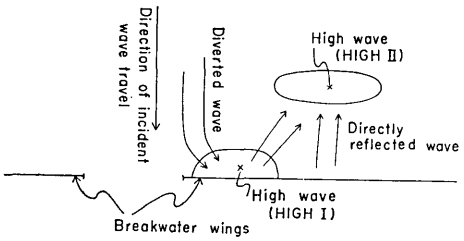

Fig. 14. Generation mechanism of high waves.

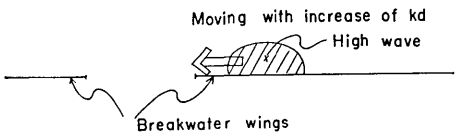

Fig. 15. Behavior of high waves for an increase of kd.

Let us next discuss the variation of phase in the windward waters (refer to Figs. 8(pw), 9(pw), 10(pw) and 11(pw)).

In the same way as that in the previous work (paper I), the diverted waves appearing in the nearby area of the breakwater gap are reflected obliquely to the offiing with accompanying rotation of waves as complementary flows (a figurative explanation is given in Fig. 43 of paper I). As kd increases from 0.1 to 1.0 (in paper I) and further from 2.0 to 5.0 (in the present work), the center of rotating waves in the adjacent part of the breakwater gap (designated by *ROTATING WAVE* (*RI*) in Fig. 43 of paper I) approaches gradually to the corner of the breakwater wing. The undulatory variation of the amplitude along the windward wall of

the breakwater wing has already been noted. Then the second high waves (designated by HIGH I′ in Fig. 42 of paper I) are interpreted as being produced as the result of a collision of the counter-rotating waves (denoted by *ROTATING WAVE* (*RI′*) in Fig. 43 of paper I) with the breakwater wing (see Fig. 16). In Figs. 8(*pw*), 10(*pw*) and 11(*pw*), a row of the centers of rotating waves run in parabolical form from the breakwater gap to the outer sea (see Fig. 17), while, in Fig. 9(*pw*) and the pictures of phase in the windward waters in paper I, such a fact cannot be definitely detected owing to the shortage of the depicted regions.

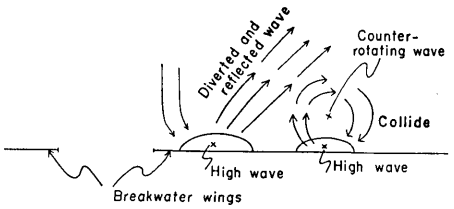

Fig. 16. Generation mechanism of the second high wave in the windward part of the breakwater wing.

Comparing Figs. 8(*aw*), 9(*aw*), 10(*aw*) and 11(*aw*) with Figs. 8(*pw*), 9(*pw*), 10(*pw*) and 11(*pw*) respectively, it turns out that the center of rotating waves corresponds to the point of the lowest amplitude, though a slight difference for two points is found due to the difficulty of obtaining the point of the lowest amplitude in the present calculation (see Fig. 18).

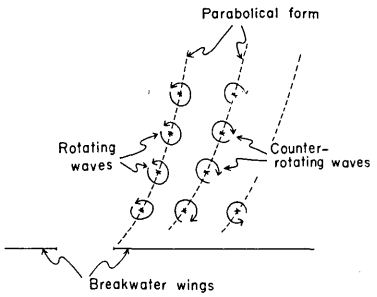

Fig. 17. Parabolical extension of rows of rotating waves in the windward waters.

We turn our attention to the behavior of the waves in the leeward waters.

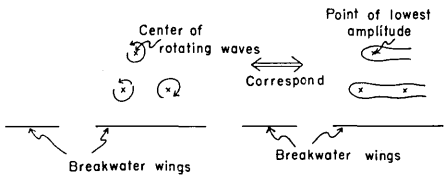

Fig. 18. Correspondence of the center of rotating waves and the point of the lowest amplitude in the windward waters.

To begin with, the variations of the amplitude (Figs. 8(*al*), 9(*al*), 10(*al*) and 11(*al*)) are treated. Through four figures, the most conspicuous feature is the appearance of mounds of the amplitude in the leeward waters of the breakwater gap which exceeds 1.0 (the amplitude of the invading waves). According to Dr. Mogi's paper[3], such an appearance of the mounds is ascertained from his experiments. In the range of small kd ($=0.1$ to 1.0) in the previous work (paper I), such a mound

3) K. MOGI, *Bull. Earthq. Res. Inst.*, **34** (1956), 267.

did not appear. As already mentioned in Section *3,2*, the mound of the amplitude increases in height as it moves away from the breakwater gap to the leeward when *kd* increases. Concerning the generation mechanism of the mound, it is interpreted as being produced as the result of the interference of the directly invading waves from the breakwater gap and the diffracted waves from the breakwater wings (refer to Fig. 19). As

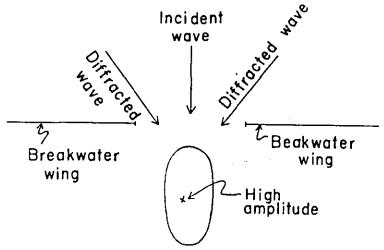

Fig. 19. Generation mechanism of the mound behind the breakwater gap.

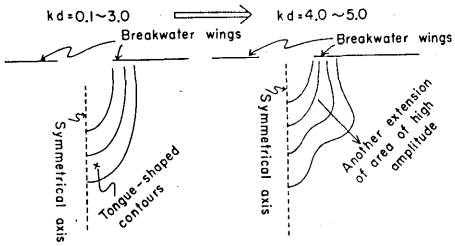

Fig. 20. Generation of the convex extension of area of high amplitude.

kd increases, a gradual extension of the region of high amplitude in the leeward waters is found which is due to the intensification of the directivity of the waves. In the range of small *kd* (=0.1 to 3.0), including the results of the previous work (Figs. 36 and 40 in paper I), the area of high amplitude is extended in a tongue-shape manner to the leeward, while, in the range of $kd=4.0$ and 5.0, such a tongue-shape is deformed to yield another convex extension of the contours, which runs obliquely to the leeward (refer to Fig. 20). An interpretation of the generation mechanism of such an oblique convex extension of the contours is that, as *kd* increases, the directivity of the waves begins to be so severe that the directly incident waves and the diffracted waves from the corners of the breakwater wings are definitely separated.

As far as the behavior of the phase of the waves in the leeward waters is concerned, the following facts are known from Figs. 8 (*pl*), 9(*pl*), 10(*pl*) and 11(*pl*). Referring to the above four figures, as *kd* increases from 2.0 to 5.0, a gradual intensification of the directivity of the waves is found. That is to say, when *kd* increases, the crest lines of the waves passing through the breakwater gap begin to run more parallel to the breakwater wings. Going away from the breakwater gap, the shapes of the crest lines are deformed to a circular form with the center at the midpoint of the breakwater gap. In the figures of the range above $kd=3.0$ (Figs. 9(*pl*), 10(*pl*) and 11(*pl*)), a sense of convergence of the waves

to the axis which runs perpendicular to the breakwater wings through the midpoint of the breakwater gap is detected (see Fig. 21).

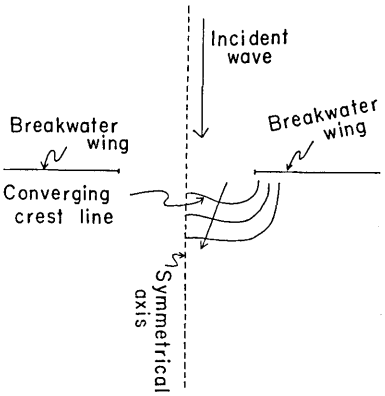

Fig. 21. Figurative explanation of converging crest lines.

3,4. Overall Variations of the Amplitude and Phase of RD Waves.

In this section, the variations of the *RD* waves in the nearby area of the breakwater gap are discussed for specified parameters $kd=0.1$, 1.0, 2.0, 3.0, 4.0 and 5.0. The pictures showing the variations of the amplitude and phase are presented, respectively, in Figs. 22(*a*), 23(*a*), 24(*a*), 25(*a*), 26(*a*) and 27(*a*) for the amplitude of $kd=0.1$, 1.0, 2.0, 3.0, 4.0 and 5.0, and also in Figs. 22(*p*), 23(*p*), 24(*p*), 25(*p*), 26(*p*) and 27(*p*) for the phase of $kd=0.1$, 1.0, 2.0, 3.0, 4.0 and 5.0, where the italic letters *a* and *p* in the brackets imply the figures relevant to the amplitude and phase. The approximations used in describing the above pictures are, respectively, the 5 th, 9 th, 11 th, 19 th, 27 th and 29 th approximations for $kd=0.1$, 1.0, 2.0, 3.0, 4.0 and 5.0.

As already mentioned in the beginning of Section 3, the *RD* waves are the waves reflected and diffracted by an obstacle, after the incident waves have arrived at the obstacle, which do not include the component of the invading waves.

Through the figures relavant to the amplitude variation of the *RD* waves (Figs. 22(*a*) to 27(*a*)), the region of large amplitude extends, in the oblique direction, from the part of the breakwater wing near the gap to the outer sea (see Fig. 28). These extensions run in the sense of the propagation of the diverted and reflected waves which take place in the nearby region of the breakwater gap (the details of which have been discussed in the previous Section *3,3*), being gradually uplifted in the direction of the incident waves with an increase of *kd* from 0.1 to 5.0. In the region facing the breakwater gap, the contours of the amplitude of the *RD* waves, when *kd* is small (Figs. 22(*a*) and 23(*a*)), take a relatively smooth circular form, while, when *kd* becomes large (Figs. 24(*a*), 25(*a*), 26(*a*) and 27(*a*)), such a circular form varies in a peculiar pattern of interference which is caused by the overlapping of the two waves reflected from the two breakwater wings. Outside

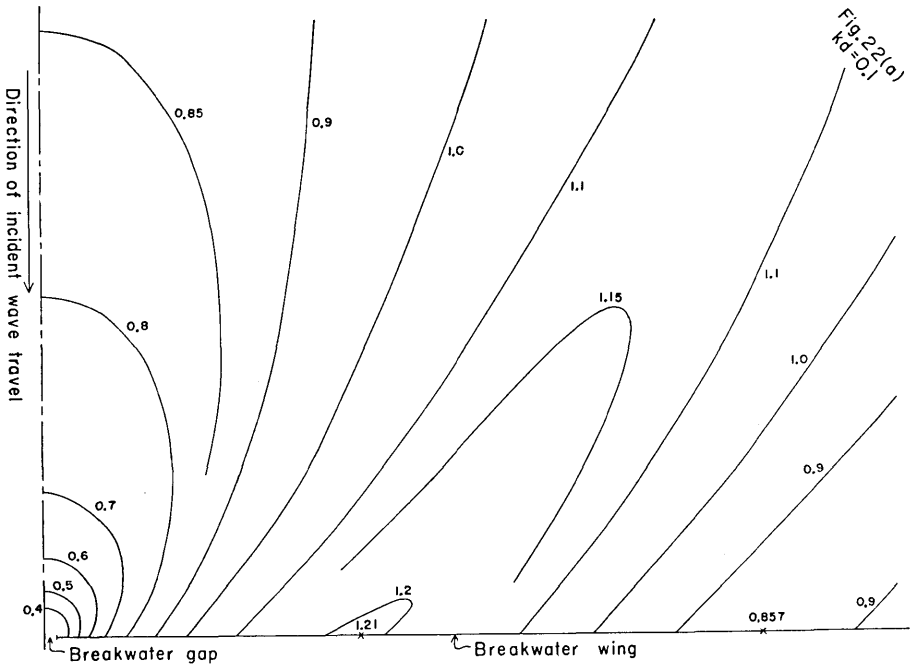

Fig. 22(*a*). Overall variation of amplitude of *RD* waves in the windward waters for $kd=0.1$. The numerals stated in the figure denote the values of $|\zeta/\zeta_0|$ which are normalized by the amplitude of the incident waves. Owing to the symmetry of the phenomenon, only the right-hand figure is depicted.

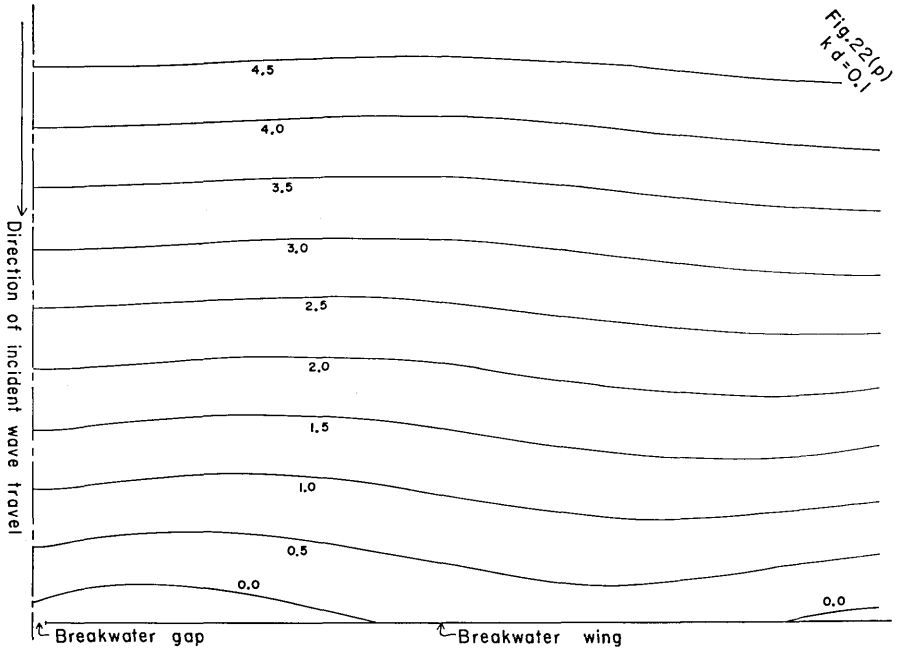

Fig. 22(*p*). Overall variation of phase of *RD* waves in the windward waters for $kd=0.1$. The numerals stated in the figure denote the values of $\arg\zeta$. Because of the symmetry, only the half figure is depicted.

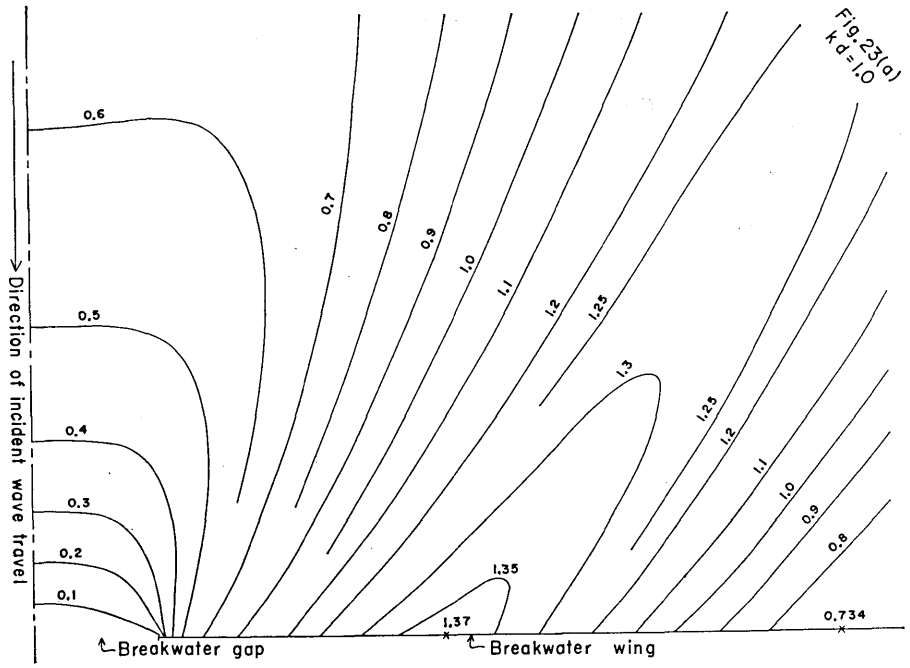

Fig. 23(*a*). Overall variation of amplitude ($|\zeta/\zeta_0|$) of *RD* waves in the windward waters for $kd=1.0$. Because of the symmetry, only the half figure is retained.

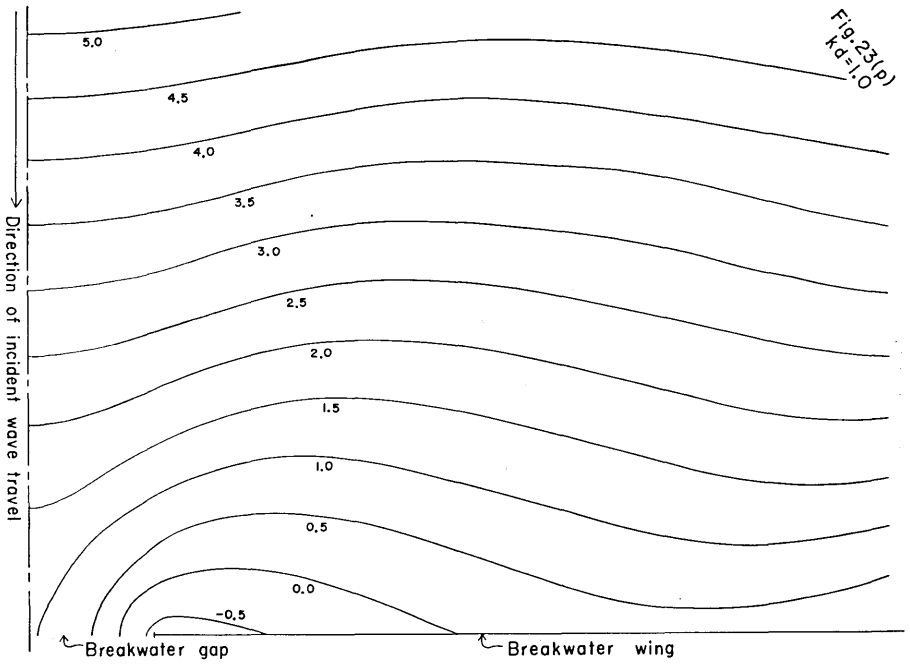

Fig. 23(*p*). Overall variation of phase ($\arg\zeta$) of *RD* waves in the windward waters for $kd=1.0$. Only the half figure is depicted.

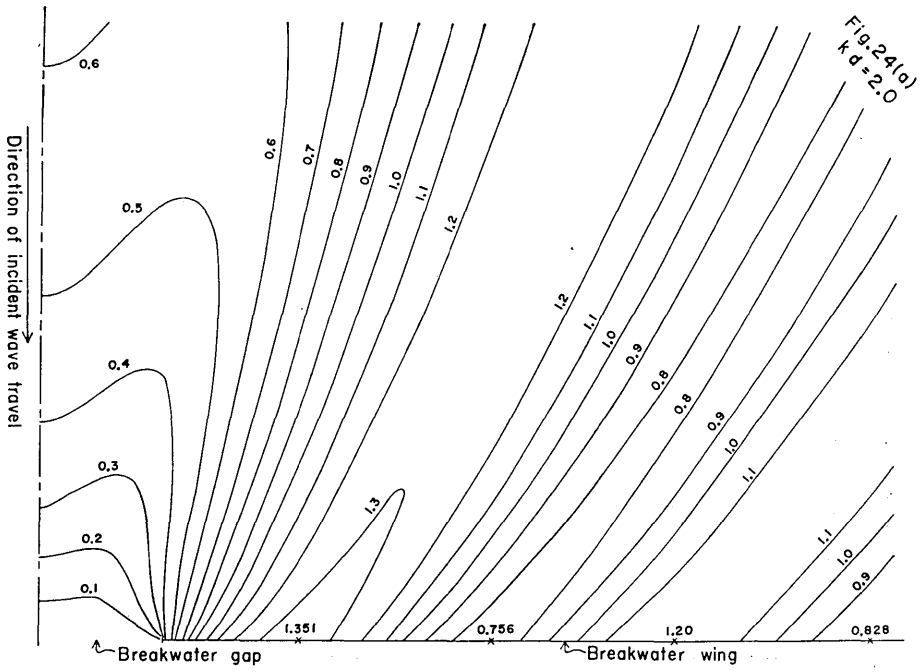

Fig. 24(*a*). Overall variation of amplitude ($|\zeta/\zeta_0|$) of *RD* waves in the windward waters for $kd=2.0$. Only the right-hand figure is depicted.

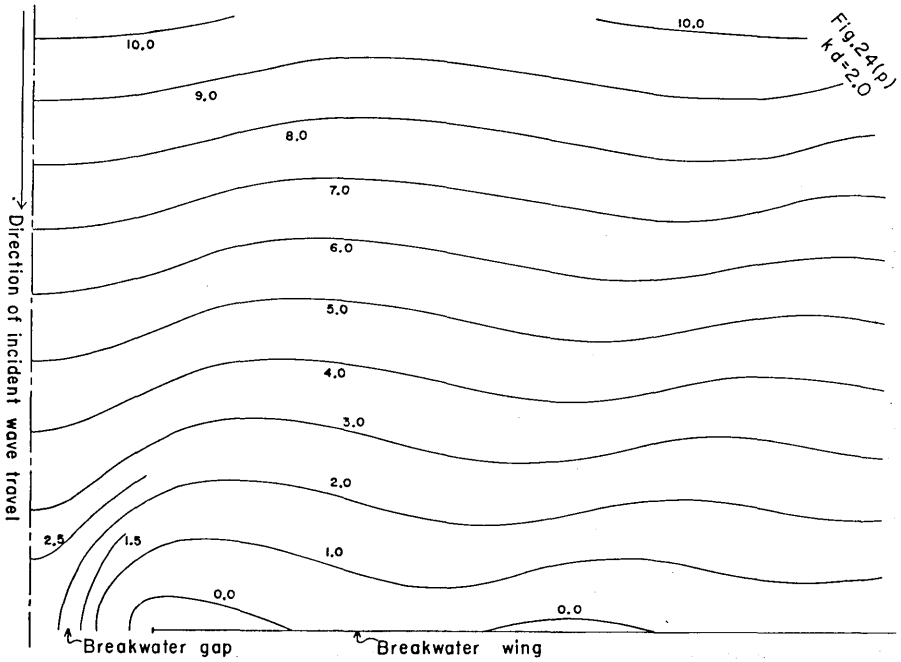

Fig. 24(*p*). Overall variation of phase ($\arg\zeta$) of *RD* waves in the windward water for $kd=2.0$. Because of the symmetry, only the half figure is depicted.

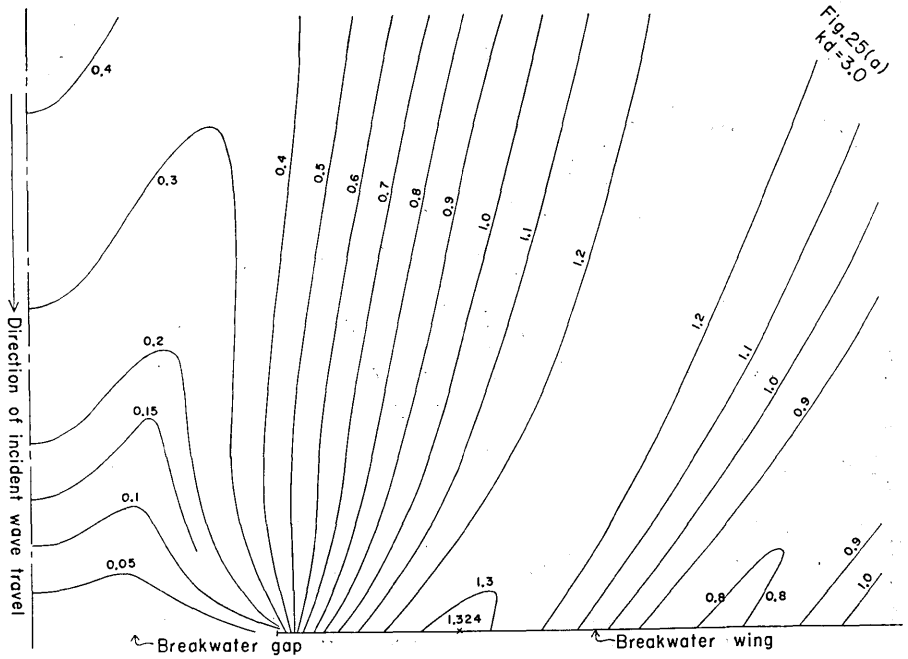

Fig. 25(*a*). Overall variation of amplitude ($|\zeta/\zeta_0|$) of *RD* waves in the windward waters for $kd=3.0$. Only the half figure is retained.

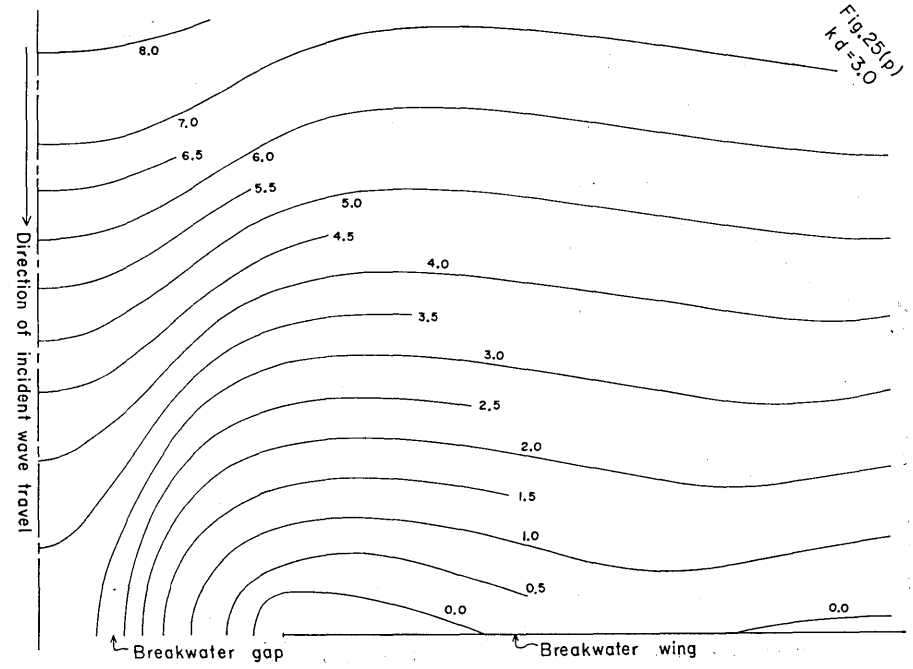

Fig. 25(*p*). Overall variation of phase ($\arg\zeta$) of *RD* waves in the windward waters for $kd=3.0$. Only the half figure is retained.

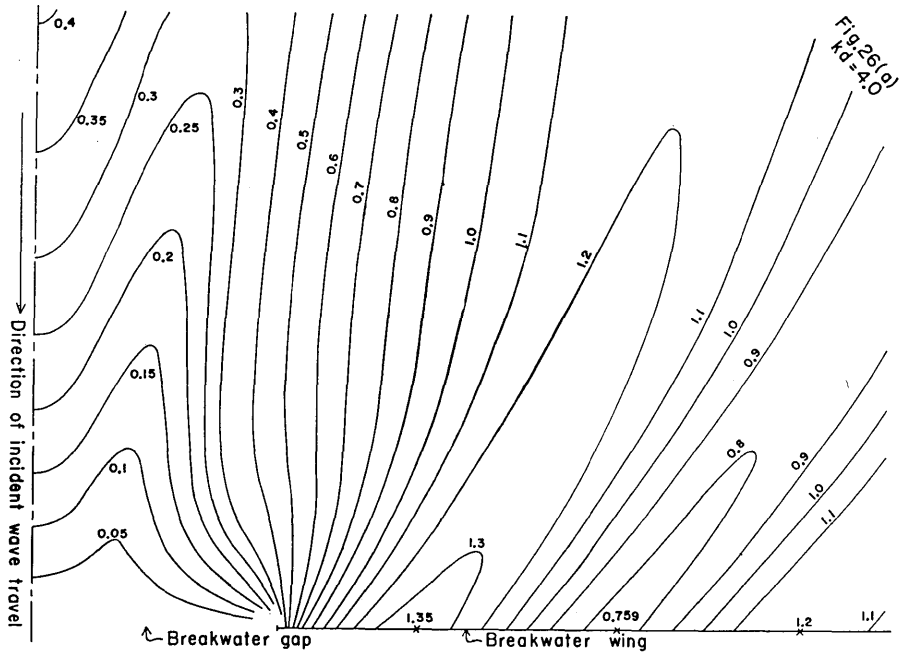

Fig. 26(*a*). Overall variation of amplitude ($|\zeta/\zeta_0|$) of *RD* waves in the windward waters for $kd=4.0$. Only the half figure is depicted.

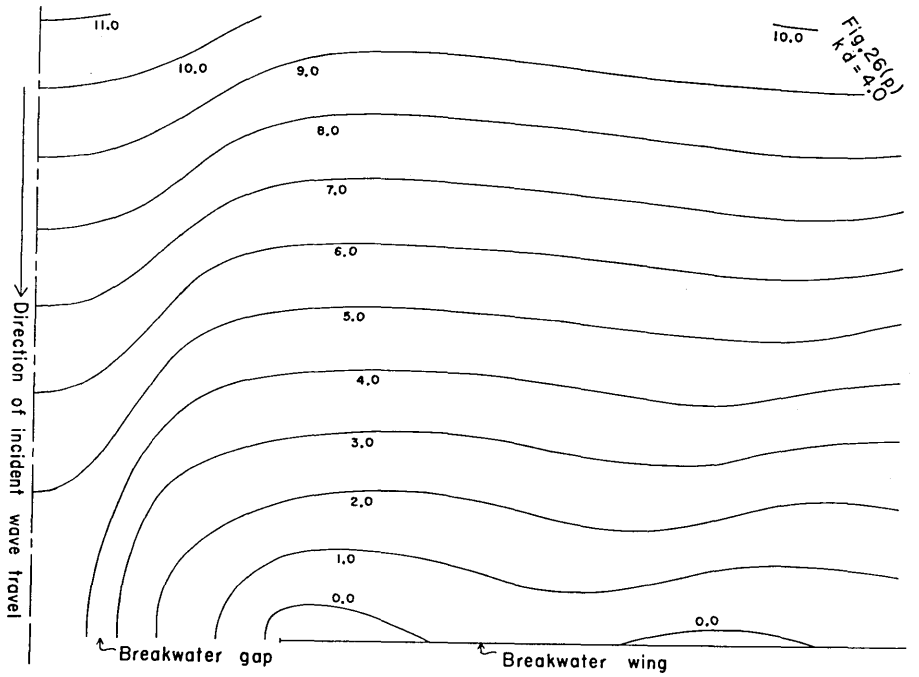

Fig. 26(*p*). Overall variation of phase ($\arg\zeta$) of *RD* waves in the windward waters for $kd=4.0$. Only the half figure is retained.

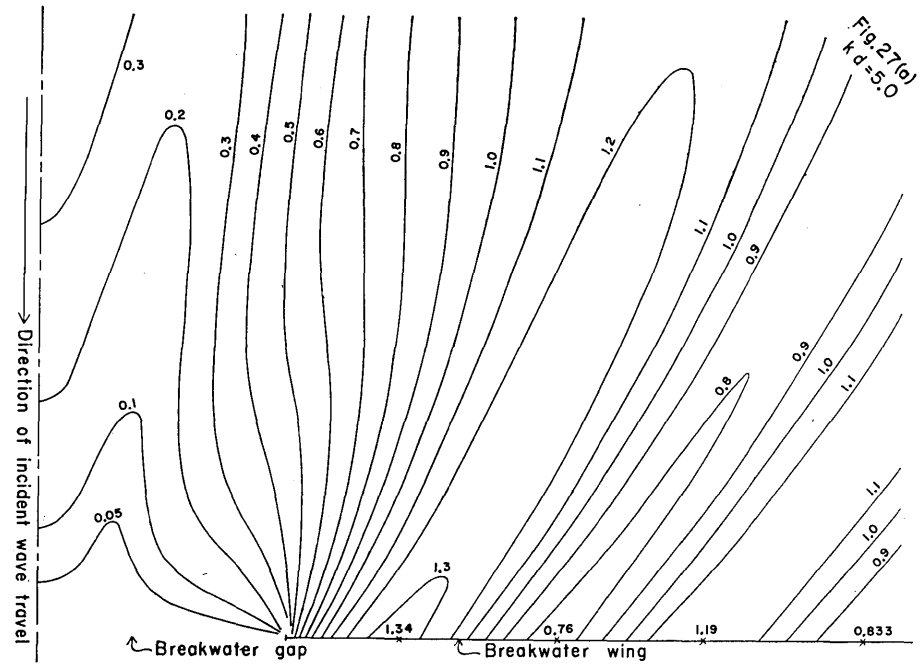

Fig. 27(*a*). Overall variation amplitude ($|\zeta/\zeta_0|$) of *RD* waves in the windward waters for $kd=5.0$. Only the half figure is depicted.

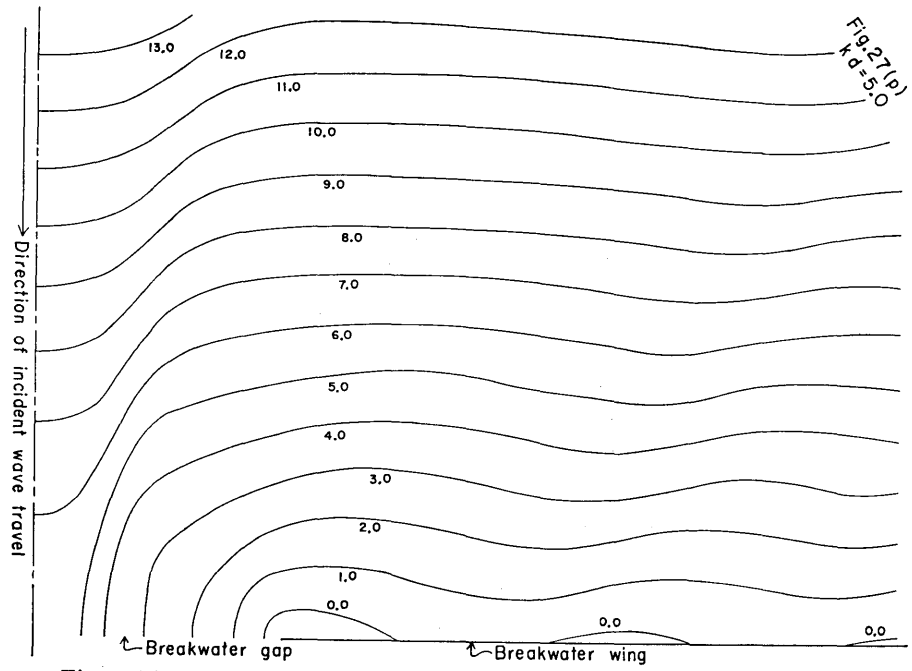

Fig. 27(*p*). Overall variation of phase ($\arg\zeta$) of *RD* waves in the windward waters for $kd=5.0$. Only the half figure is retained due to the symmetry.

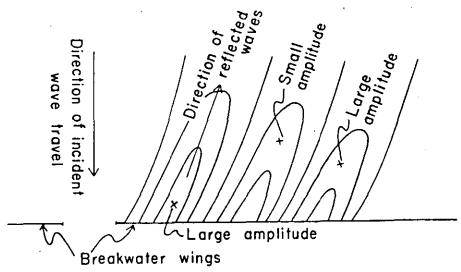

Fig. 28. Oblique extensions of the regions of large and small amplitudes of *RD* waves.

the aforementioned stripe of large amplitude, another stripe of small amplitude is found in Figs. 22(a) to 27(a). Running from the breakwater gap along the wing, these two kinds of stripes of high and low amplitudes appear alternately with decreasing amplitude (refer to Fig. 28).

Finally, our attention is focussed upon the behavior of the phase of the *RD* waves.

Referring to Figs. 22(p), 23(p), 24(p), 25(p), 26(p) and 27(p) which show the variations of phase of *RD* waves in the windward waters, the following facts are exposed. In the above six figures, a prevailing feature is the oblique crest lines which denote the existence of diverted and reflected waves near the corner of the breakwater wing (refer to Fig. 29). As kd increases, the origin of the diverted and reflected waves moves on toward the corner of the wing. As a component of the counter-rotating waves, weak oblique reflected waves appear in the counter-direction of the diverted and reflected waves as the complementary flow (refer to Fig. 30). In the frontal area of the breakwater gap, a converging sense of the crest lines is found in Figs. 23(p) to 27(p) (except for Fig. 22(p)), which is interpreted as causing large amplitude in the above region (refer to Fig. 31).

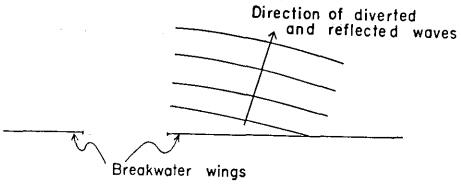

Fig. 29. Appearance of obliquely reflected waves.

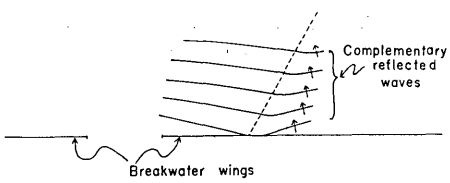

Fig. 30. Generation of complementary reflected waves.

After a simple algebraic manipulation, the expression of the *RD* wave in the buffer domain (the case for $j=2$ in (30)) is reduced to the following (the expression (23) is used):

$$\phi_{rd}^{(2)} = i\cdot\phi_0 \sin ky + \sum_{m=0}^{\infty} \phi_2^{(2m+1)} J_{2m+1}(kr) \sin (2m+1)\theta\,. \tag{33}$$

From the above equation, the relation

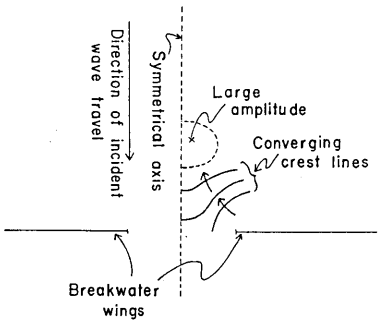

Fig. 31. Convergence of *RD* waves in front of the breakwater gap.

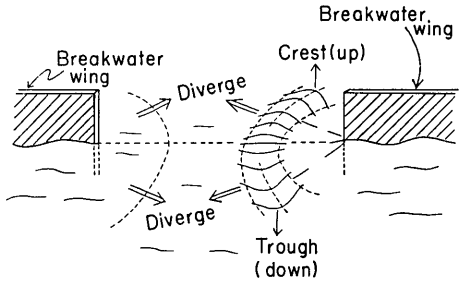

Fig. 32. Illustration of *RD* waves around the breakwater gap.

$$\phi_{rd}^{(2)}(r, \theta) = -\phi_{rd}^{(2)}(r, -\theta) ,$$

is found, that is to say, $\phi_{rd}^{(2)}$ is an odd function with respect to θ. This feature is shown in Fig. 32.

---

40. 防波堤のまわりにおける長波 (垂直入射の場合) [II]

地震研究所　桃　井　高　夫

本論説は同じ題名のもとにおこなわれた前研究の続きである．基本方程式は前報告と異り，速度ポテンシャルで表現される方程式である（前報告では長波の方程式が用いられている）．計算された kd (k: 進入波の波数，d: 防波堤開口部の半分の長さ）の範囲は *RST* (resultant) 波に対して 2.0 から 5.0, *RD* (reflected and diffracted) 波に対して 0.1 から 5.0 までである．そして kd の変化に対するこれらの波の変化の状態が防波堤の近傍領域で論じられている．